AD_____

Award Number: W81XWH-07-1-0305

TITLE: Innovative Microsystems: Novel Nanostructures to Capture Circulating Breast Cancer Cells

PRINCIPAL INVESTIGATOR: Yitshak Zohar, PhD
James C. Baygents, PhD
Roberto Guzman, PhD
Ronald L. Heimark, PhD
Joyce A. Schroeder, PhD

CONTRACTING ORGANIZATION: University of Arizona
Tucson, AZ 85721

REPORT DATE: May 2009

TYPE OF REPORT: Annual

PREPARED FOR: U.S. Army Medical Research and Materiel Command
Fort Detrick, Maryland 21702-5012

DISTRIBUTION STATEMENT:

☒ Approved for public release; distribution unlimited

REPORT DOCUMENTATION PAGE

Form Approved
OMB No. 0704-0188

1. REPORT DATE *(DD-MM-YYYY)*	**2. REPORT TYPE**	**3. DATES COVERED** *(From - To)*
01-06-2009	Annual	23 April 2008 – 22 April 2009

4. TITLE AND SUBTITLE

Innovative Microsystems: Novel Nanostructures to Capture Circulating Breast Cancer Cells

5a. CONTRACT NUMBER

5b. GRANT NUMBER
W81XWH-07-1-0305

5c. PROGRAM ELEMENT NUMBER

6. AUTHOR(S)

Yitshak Zohar
James Baygents
Roberto Guzman
Ron Heimark
Joyce Schroeder
Email:zohar@ame.arizona.edu

5d. PROJECT NUMBER

5e. TASK NUMBER

5f. WORK UNIT NUMBER

7. PERFORMING ORGANIZATION NAME(S) AND ADDRESS(ES)

University of Arizona

Tucson, AZ 85721

8. PERFORMING ORGANIZATION REPORT NUMBER

9. SPONSORING / MONITORING AGENCY NAME(S) AND ADDRESS(ES)

US Army Medical Research & Materiel Command

Fort Detrick, Maryland 21702-5012

10. SPONSOR/MONITOR'S ACRONYM(S)

11. SPONSOR/MONITOR'S REPORT NUMBER(S)

12. DISTRIBUTION / AVAILABILITY STATEMENT

Approved for public release; distribution unlimited

13. SUPPLEMENTARY NOTES

14. ABSTRACT

The goal of this project is to develop a microsystem for sorting metastatic breast cancer cells from a heterogeneous suspension of cells circulating in the blood stream. Conceptually, the technique requires the transformation of a distinguishing biochemical characteristic of the target cells, such as up-regulated cadherin phenotype, into a mechanical or electrical that makes it possible to selectively manipulate the cells on the microscale. The project includes developments of a model system of cells to evaluate cadherin-mediated cell sorting and an integrated bio-functional microfluidic system to capture target cells from heterogeneous suspensions of cells. We have succeeded in the transfection of MDA-MB-231 cells with an N-cadherin expression vector deriving a homogeneous population. An anti-N-cad functionalized surface has been shown to capture N-cad expressing prostate cancer cells (PC3N) with high degree of selectivity. An assay to characterize and a technique to control the amount of immobilized anti-N-cad antibodies on surfaces have been developed to maximize the cell capture efficiency. Microchannels with anti-N-cad functionalized surfaces have been fabricated. Under flow conditions, the capture rate is poor; however, after 15min of incubation time, the capture rate is high. Once captured, the cell/surface adhesion bond is strong enough to sustain high flow-induced shears stress.

15. SUBJECT TERMS

Circulating breast cancer cells, Microfluidics, Nanostructures, Surface derivatization

16. SECURITY CLASSIFICATION OF:			**17. LIMITATION OF ABSTRACT**	**18. NUMBER OF PAGES**	**19a. NAME OF RESPONSIBLE PERSON**
					USAMRMC
a. REPORT	**b. ABSTRACT**	**c. THIS PAGE**	UU	45	**19b. TELEPHONE NUMBER** *(include area code)*
U	U	U			

Standard Form 298 (Rev. 8-98)
Prescribed by ANSI Std. Z39.18

Table of Contents

Page

Introduction

The goal of this project is to develop a microsystem for continuous sorting of target breast cancer cells from a heterogeneous suspension of cells. Conceptually, the technique requires the transformation of a distinguishing biochemical characteristic of the target cells, such as up-regulated cadherin phenotype, into a mechanical, electrical or magnetic property that makes it possible to selectively manipulate the cells on the microscale. Such manipulations, then, permit one to continuously flow the entire suspension through a network of nanostructures, sorting out the target cells by taking advantage of their unique physical feature. The project involves the following major steps:

- Determining the parameters of cadherin-mediated adhesion for sorting a single group of cancer cells from a mixed population including the development of a model system of cells to evaluate cadherin-mediated cell sorting on MEMS, and estimating the sensitivity of cadherin-mediated cell capture for an *in vivo* system (SCID mice).
- Fabricating bio-functional microchannels, about 100μm in height, to capture target cells including immobilization of prescribed patterns of cadherin counter-ligands within microchannels etched into silicon, as well as evaluating the effectiveness of these patterns in capturing target cells from flowing suspensions.
- Building an integrated microdevice to select circulating cancer cells from heterogeneous suspensions of cells such as in blood.

The first two steps are formulated to lay the foundation for the third step, which involves fabrication of microdevices with integrated networks of microchannels, fluid reservoirs, pumps and the functionalized surface regions.

Body

The results obtained during this reporting period are classified into three main topics: (i) specific binding of Cancer Cells using a microchamber array functionalized with antibodies, (ii) kinetics of specifically captured cancer cells in antibody-functionalized microchannels, and (iii) detachment of captured cancer cells under flow acceleration in functionalized microchannels.

I - Specific Binding of Cancer Cells Using a Microchamber Functionalized with Antibodies

The interaction between cancer cell surface antigens and antibody-functionalized surfaces is a complicated process depending on numerous parameters. In order to exercise better control over several key variables, a microfluidic device consisting of a 5×5 microchamber array has been designed as sketched in Figure 1a. The tight tolerance of each microchamber volume provides a convenient tool for counting biding events under fine-controlled conditions.

The fabrication starts with thermal growth and patterning of a 3000Å-thick oxide on a silicon wafer, 500μm in thick, to serve as a mask for the Deep Reactive Ion Etching (DRIE) process. The oxide film is stripped away after etching a 5×5 chamber array; each chamber is 50μm in depth and 1mm×1mm in area. The substrate is then re-oxidized to form a 3000Å-thick oxide layer to serve as a seed layer immobilizing antibodies. A photograph of a fabricated microchamber array is shown in Figure 1b. The oxide surface of the fabricated chamber array is functionalized with a bio active layer. The hydroxyl groups are silanated in 1% (vol./vol.) 3-aminopropyltriethoxysilane (APTES from Sigma) - acetone solution for 30 minutes at room temperature. The APTES-coated surface is activated with 2% (vol/vol) glutaraldehyde (Sigma) in water for 2 hours at room temperature to promote a Schiff-base reaction. Recombinant protein G from *E. coli* (Zymed Lab Inc.) 50 μg/ml in Ca- and Mg-free phosphate-buffered saline (CMF-PBS), is incubated on the activated surface for 3 hours at 4ºC. In order to block excess of silane sites, bovine serum albumin (BSA from Sigma) solution (2mg/ml in CMF-PBS) is incubated on the surface for 1 hour at room temperature. Various antibodies, at 100 μg/ml in CMF-PBS, are finally incubated on the protein G layer at room temperature for 1 hour. The antibodies used in this work include anti-N-cadherin (IgG1, clone GC-4 from mouse, Sigma), anti-E-Cadherin (from mouse, Invitrogen), and mouse IgG (Sigma).

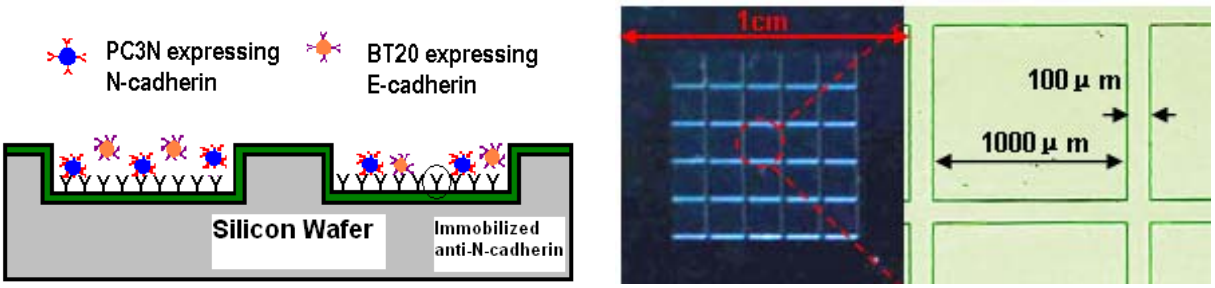

(a) (b)

Figure 1, A microchamber array: (a) a schematic device cross-section designed for the capture of target cancer cells on an antibody-functionalized surface, and (b) a photograph of a fabricated microdevice with an enlarged image of a single chamber, 1000x1000μm^2 in area and 50μm in depth; the width of the separation wall is 100μm.

The N-cadherin expressing PC3N prostate cancer cell line was grown in 1×DMEM/F12 (Dulbecco's modified Eagle's medium with 1:1 Ham's F12 medium, Invitrogen) with 10% fetal bovine serum (FBS) (Omega Scientific) and 1% penicillin-streptomycin (Cellgro). The E-cadherin expressing BT20 breast cancer cell line was grown in Eagle's Minimum Essential Medium (EMEM from ATCC) with 10% FBS and 1% penicillin-streptomycin. The cadherin-11 expressing MDA-MB-231 breast cancer cell line was grown maintained in RPMI 1640, with L-glutamine (Cellgro) with 10% FBS and 1% penicillin-streptomycin. All the cell lines were maintained at 37°C in 5% CO_2 in humid environment. Prior to experiments, the growth medium was aspirated and the cells were incubated with 4mM ethylenediamine-tetraacetic acid (EDTA) in CMF-PBS for 30 minutes for detachment. After centrifugation and solution removal, the cells are re-suspended in CMF-PBS. In the mixture experiment, to distinguish between cells, the cells were incubated with Celltracker (Invitrogen) 4.5uM in Dulbecco's Phosphate-Buffered Saline (D-PBS) for 30 minutes before EDTA detachment.

The effects of several key incubation parameters on the interaction between the target cells and the functionalized surface have been studied. The effect of cell concentration and incubation time on the cell capture rate was first tested. A suspension of PC3N cells, with concentration in the range of 10^4-2.5x10^5/ml, was incubated on anti-N-cadherin functionalized micro-devices. After each certain incubation time, the devices were washed and the captured cells were counted. The incubation time includes the cell sedimentation time and cell-surface binding time. For every fixed incubation time, the area density of captured PC3N increases linearly with the suspended cell concentration as shown in figure 2a. The captured PC3N cell density is plotted in Figure 2b as a function of the incubation time for various cell suspension concentrations. For each given concentration, the captured cell density increases exponentially with incubation time. The asymptotic density level of the captured cancer cells on the functionalized surface increases linearly with the cell-suspension concentration. Furthermore, the time constant characterizing the exponential increase in cell density also increases with the cell concentration. For example, 15min incubation time was needed for the cell density to level off for cell concentration of 10^4cells/ml, while it took about 30min incubation time for cell concentration of 10^5cells/ml.

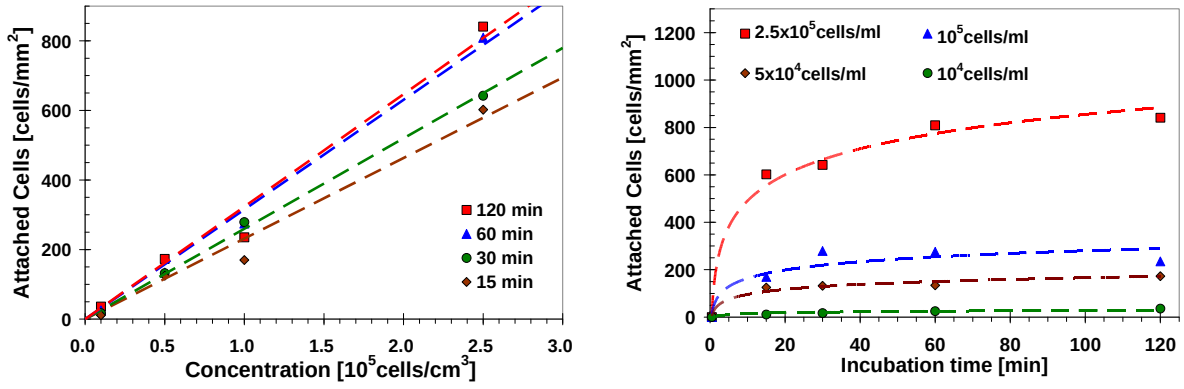

(a) (b)

Figure 2, PC3N cell density, captured on an anti-N-cadherin functionalized surface, as a function of: (a) cell suspension concentration, and (b) incubation time.

The antigen–antibody binding is temperature-dependent; therefore, different cell capture rates are expected under various ambient temperatures. At temperatures around 37°C, though, the

immobilized antibody-cell receptor interaction could be affected by receptor internalization. Thus, cells at 37°C were treated with sodium azide (NaN_3) prior to detachment to prevent receptor internalization. PC3N cell suspensions, with a fixed concentration of 10^5cells/ml, were incubated on anti-N-cadherin functionalized micro-chambers under ambient temperatures varying from 4°C to 37°C. The ratio between the number of captured cells and the number of initially suspended cells, defined as the capture ratio, is plotted in Figures 3a and b as a function of incubation time and ambient temperature, respectively. Cells without sodium azide treatment were also incubated at 37°C for comparison. The cell captured rate at 4°C ambient temperature is practically zero for an incubation time up to 60min. At higher ambient temperatures, the capture ratio is 90% after 15min incubation time. No significant difference in capture rate is observed between incubation at 25°C and 37°C, and no effect due to sodium azide treatment is detected.

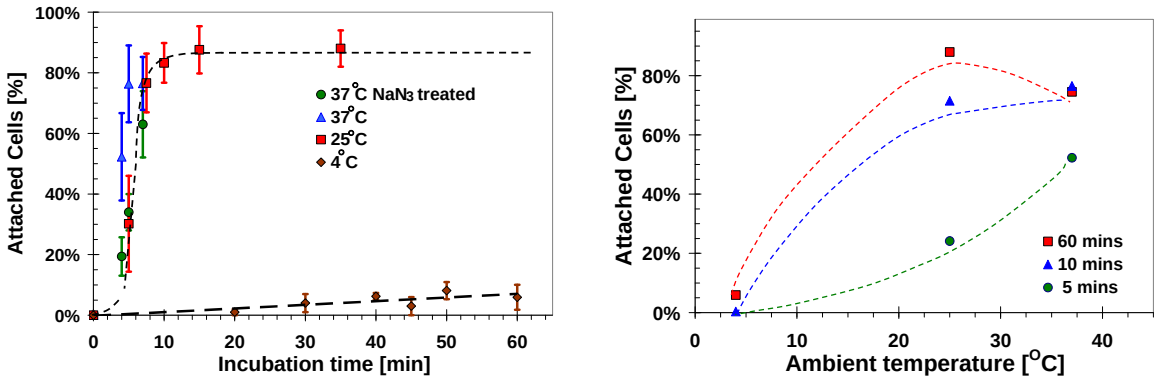

(a) (b)

Figure 3, PC3N cells captured on an anti-N-cadherin functionalized surface, as a function of: (a) incubation time, and (b) ambient temperature.

Cancer cell specific binding to a functionalized surface primarily depends on the surface properties. Thus far, the experimental results indicated high capture efficiency of N-cadherin expressing PC3N cancer cells, almost 100%, on an anti-N-cadherin functionalized surface. In order to test the specificity of the cell-surface interaction, identical PC3N cell suspensions ($5x10^5$cells/ml) were incubated on three surfaces with different coatings: (i) anti-N-cadherin, (ii) mouse IgG as a negative control, and (iii) SiO_2. The measured capture ratios are compared in Figure 4a. The capture rate of PC3N cell on the anti-N-cadherin surface is about 100%, the capture rate of the same cells on mouse IgG and SiO_2 surfaces is only 5% and 0.2%, respectively. This demonstrated that N-cadherin expressing cells have high affinity to an anti-N-cadherin functionalized surface. In order to demonstrate that this characteristic is not limited to PC3N cells, the experiments were repeated for E-cadherin expressing BT20 cancer cells. Cell suspensions, at 10^5cells/ml concentration, were incubated on surfaces functionalized with: (i) anti-E-cadherin, (ii) anti-N-cadherin, (iii) mouse IgG, and (iv) SiO_2. The measured capture rates are compared in Figure 4b. Indeed, high capture rate of nearly 100% is observed only for BT20 cell incubation on an anti-E-cadherin surface, while the rate over other surfaces is less than 10%. Thus, a functionalized anti-N-cadherin surface binds with high selectivity only N-cadherin expressing cells, indicating that the surface has a high degree of specificity.

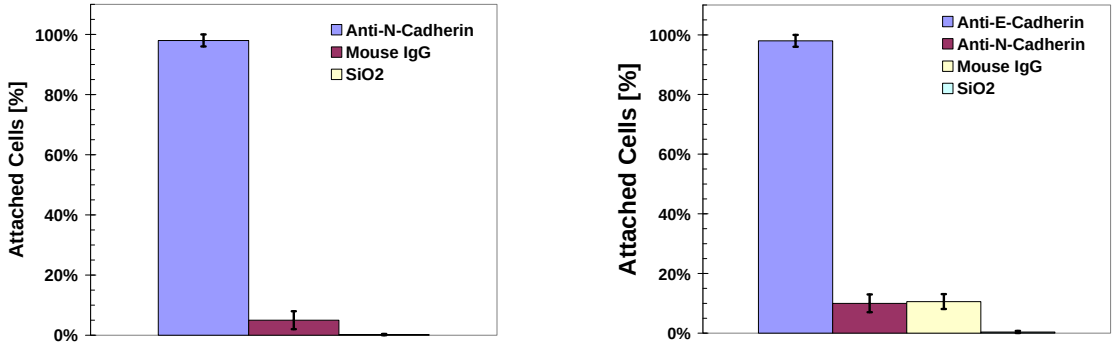

(a) (b)

Figure 4, Measured capture rates on surfaces with different coatings for: (a) PC3N, and (b) BT20 cells.

The selectivity of binding target cancer cells only on a certain functionalized surface was tested using different cell types on similarly treated surfaces. Suspensions, at the same concentration of 10^5cells/ml, of three cancer cell types: (i) N-cadherin expressing PC3N, (ii) E-cadherin expressing BT20, and (iii) Cadherin-11 expressing MDA-MB-231 cells, have been incubated for 60min on anti-N-cadherin functionalized surfaces. The capture rates are plotted in Figure 5a. Clearly, about 100% of the N-expressing PC3N cells were captured, while about 10% and only 1% of the MDA-MB-231 and BT20 cells were respectively captured. This confirms that not only the anti-N-cadherin functionalized surface has high affinity to N-cadherin expressing cells, but it also has very low affinity to other cancer cells expressing receptors different from N-cadherins.

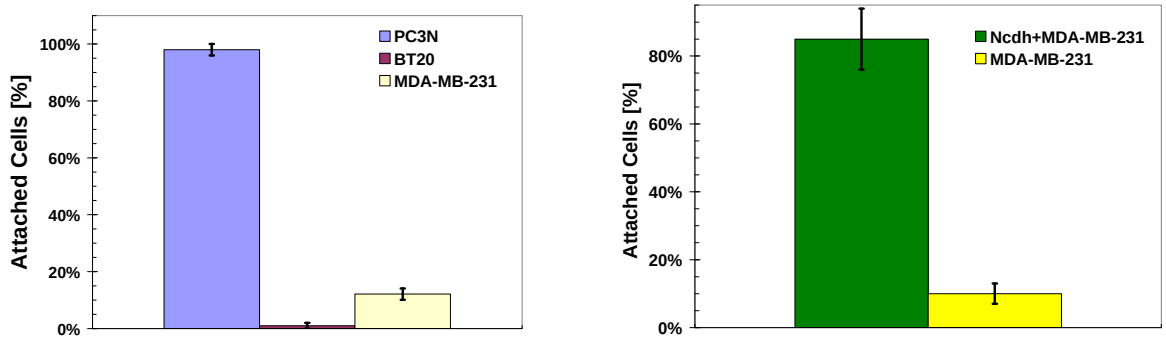

(a) (b)

Figure 5, Capture rates of (a) different cell lines, and (b) Ncdh+MDA-MB-231 and MDA-MB-231 on anti-N-cadherin surfaces.

In studying the effect of cell type on specific binding to a functionalized surface, changing the cell type is necessarily accompanied changes in other cell properties. Thus, it is important to compare binding of cells identical in all properties except their membrane receptors to categorically eliminate these modified properties as the cause for the observed poor cell affinity. MDA-MB-231 cells, normally expressing cadherin-11, were transfected with N-cadherin to perform such an experiment. Suspensions of both cell types: the transfected Ncdh+MDA-MB-231 and parental MDA-MB-231 at a 10^5cells/ml concentration were suspended on anti-N-cadherin functionalized microchambers. The corresponding capture rates are compared in Figure 5b. The capture rate of N-cadherin expressing cells is above 85%, while only 10% of the cadherin-11 expressing cells are captured. Hence, the high binding specificity to the functionalized surfaces is primarily due to the cell membrane receptors.

II – Kinetics of specifically captured Cancer Cells in an Antibody-Functionalized Microchannel

Experiments have been conducted to capture target cells from a suspension flow with the aim of isolating circulating tumor cells (CTCs) from the blood stream. Prepared cell suspensions are driven through anti-EpCAM functionalized microchannels at different flow rates which are controlled by a syringe pump. The microchannel fabrication process and the immunoassay used for functionalizing the channel with antibodies have been detailed in the previous report. Two types of cancer cells, prostate and breast, are utilized in the cell attachment experiments. PC3N prostate cancer and MDA-MB-231 breast cancer cell lines are maintained as described in Section I. All experiments are conducted and monitored using a probe station (Signatone S-1160) equipped with a microscope (Motic microscope PSM-1000), a CCD camera and a DVD recorder (Panasonic DMR-E85H) for further data processing. The prepared cancer cell suspension is loaded into an antibody-functionalized microchannel using a syringe pump (Harvard apparatus PhD 2000). Once the cell suspension is loaded, the number of cells present in the microchannel is then counted to determine the initial condition. Dilute cell suspensions at a concentration below 5×10^5 cells/ml have been used in all experiments ensuring that all cells present in the microchannel contact the channel surface with minimum cell-cell interaction. After the cell sample is loaded, unbound cells are removed by flushing 1×PBS through the microchannel at 8μl/min. Most of the data in this report are given in terms of volume flow rate, Q; dividing Q by the channel cross-sectional area yields the average flow velocity, $U_{avg}=Q/(W\cdot H)$.

Prepared cell suspensions are driven through anti-EpCAM functionalized microchannels at different flow rates which are controlled by the syringe pump. Cell receptor-ligand interaction requires a certain time to attain a strong bond. Although attempts to capture moving cancer cells under a high flow rate have not been successful, capture of cells at a relatively low flow rate has been demonstrated. To test the effect of flow rate MDA-MB231 and PC3N cell samples have been driven through anti-EpCAM functionalized microchannels at room temperature and under different flow rates. The cell suspension is loaded using the syringe pump and the number of cells present in the microchannel is then counted (N_o). A washing buffer of PBS is then used to flush the microchannel for 5min at a flow rate of 8μl/min to remove un-bounde cells. The number of the remaining cells (N_T) which are firmly attached to the functionalized surface is counted after channel washing for each tested flow rate. The fraction of the initial number of cells loaded into each channel that are captured cells is plotted in Figure 6. All curves start from unity as all cells can be captured at low flow rate. This is because by following slow fluid motion, the cell receptor has enough time to establish a strong bond with the immobilized antibody. By increasing the flow rate the fraction of captured cells decreases gradually towards zero, indicating no capture. If all cancer cells are identical, i.e. having the same number of binding sites each requiring the same bond formation time, then all cells should be captured up to the highest flow rate above which the hydrodynamic force overcomes the adhesion force. However, cells have different sizes and receptor binding strength such that the capture ratio smoothly decreases and continuously approaches zero instead of obeying a sharp step function. A simple mathematical model is used to fit to the capture efficiency versus applied flow rate,

$$\frac{N_T}{N_o} = \exp\left[-\left(Q/Q_c\right)^b\right] \quad (1)$$

Where Q_c is the critical flow rate, about 3.5μl/min for both cell lines and b is the exponential index controlling the sharpness which equals 3.5 for MDA-MB-231 and 5.5 for PC3N.

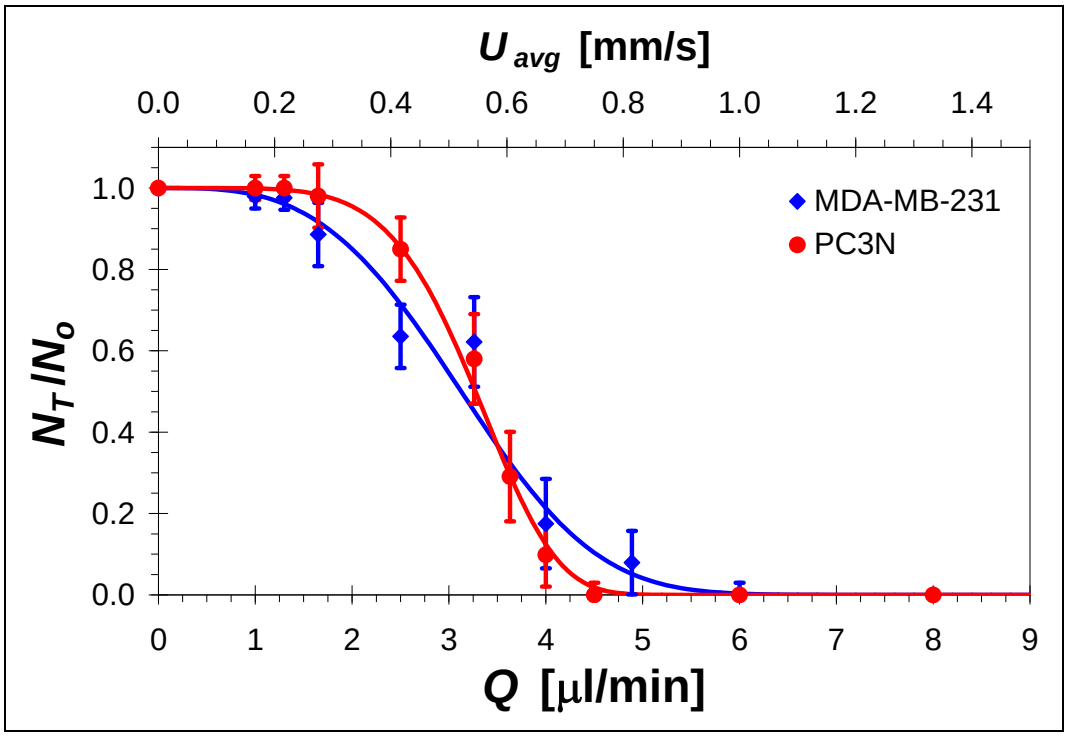

Figure 6, The capture efficiency of CTCs, MDA-MB-231 (blue) and PC3N (red) from homogeneous suspensions as a function of the applied flow rate.

Capturing of cancer cells depends on the hydrodynamic driving force and the encounter time for receptor-ligand interaction. Since cells move at a higher speed with increasing flow rate, the location to establish a successful and tight bond will also be affected by flow rate. To study the captured cell distribution, a fixed volume of cell suspension (10μl) is driven through the microchannel with different flow rates and the cell distribution is then photographed under a microscope. When the driving flow rate is low (Q=1μl/min), a fraction of the cells are already captured around the inlet location prior to entering the microchannel. Downstream of the inlet, the number of captured cells increases dramatically and reaches a maximum at x=1.5mm. Further downstream, the number of captured cell decreases rapidly within few millimeters. Even further downstream, the number of captured cells approaches zero and almost no cell capture is observed between x=8mm and 20mm. At a higher flow rate (Q=3.26μl/min), almost no cells are captured near the inlet location. A fraction of cells start to be captured in the microchannel around 1.5mm but the number of captured cells is significantly less compared to the results with a low flow rate. Moreover, instead of showing a rapid drop, the number of captured cells indeed keeps a similar value downstream of x=6mm. The number of captured cells finally decreases to zero around x=15mm.

Each rolling cell in fact requires a certain time to form a tight bond with the immobilized ligand on the microchannel surface. With a higher flow rate, cells roll longer distances before a tight bond is established. Therefore, the capture peak location is affected by the flow condition as shown before. Since cells are rolling with different speeds compared to the bulk flow due to the wall effect in the microchannel, the cell rolling velocity U_{cell} is more suitable to describe the cell motion instead of bulk flow velocity U_{avg}. Therefore, the cell rolling velocity is measured from

the recorded video with a careful selection of the rolling population by a Matlab image processing program. More than 20 individual cells are measured for each flow rate and the cell rolling velocity is found to increase linearly with the flow rate.

To find the proper time and length scales, different flow rates were tested to drive cell suspensions through the functionalized microchannels. The location of maximum capture x_p is extracted carefully from microscopy images through the entire channel. Plotting x_p as a function of U_{cell} provides a time scale t_c of about 85s. The value of t_c represents the average time for a cell to roll on the antibody coated microchannel before coming to a complete stop. To obtain a length scale from the time scale t_c, a characteristic velocity is required. Using the critical flow rate Q_c identified in the capture efficiency curve, Figure 6, the corresponding critical cell rolling velocity U_c of about 147μm/s is selected. The characteristic length scale is then calculated by multiplying U_c by t_c to obtain ξ=12.5mm. The calculated characteristic length ξ represents the rolling length for an average cell prior to capture.

The spatial pattern of cell capture is in fact a single-tailed distribution because x is bounded and defined only for positive values. The variation of the capture location x can be described as the product of independent and random factors. Hence, a log-normal distribution is suitable to model the spatial distribution in a microchannel. The log-normal probability density function g is given as follows:

$$g(\tilde{x};\mu,\sigma)=\frac{1}{\tilde{x}\sigma\sqrt{2\pi}}\exp\left[-\frac{(\ln(\tilde{x})-\mu)^2}{2\sigma^2}\right] \quad \text{and} \quad \tilde{x}=\frac{x}{\xi} \tag{2}$$

Where μ and σ are the mean and standard deviation, respectively, of the capture location's natural logarithm and will be determined by fitting the model to experiment data. ξ is the characteristic length calculated in the last paragraph. Since the integral of the g function from 0 to ∞ is equal to unity, experimental data $n(x)$ should be normalized as follows:

$$\tilde{N}=\frac{\xi\cdot n(x)}{N_T} \tag{3}$$

The experimental data and analytical results based on Equation 2 are plotted in Figure 7. The proposed log-normal probability density function closely fits the experimental data. It is apparent from the shape of the distribution that there are two groups which are separated at Q_c as a reference. When the flow rate is very low compared to the critical flow rate ($Q<<Q_c$), a distinctive sharp peak is observed in Figure 7a. The maxima are located within half of a characteristic length (ξ) of the inlet. Also, the peaks gradually shift downstream with increasing flow rate. After the peak, the capture density rapidly drops to zero. Almost all loaded cells are captured in a short distance; about one characteristic length ξ from the inlet. That implies a high capture efficiency in this range of flow rates. In this range of flow rates, the relative motion between cell receptors and ligands is extremely small. Furthermore, the capture efficiency remains approximately constant within experimental error. Therefore, in the limit of $Q<<Q_c$, the capture of cancer cells is very similar to the situation with the static condition (no flow, $Q\rightarrow 0$). Hence, the capture kinetics is dominated by the receptor-ligand interaction.

When the flow rate increases to a moderate level ($Q\approx Q_c$), the hydrodynamic force on the cell becomes comparable to the receptor-ligand interaction. Since a larger hydrodynamic force is

exerted on the cell, the cell rolling motion is larger and consequently, receptor-ligand interaction is suppressed. The spatial distribution in this transition region is depicted in Figure 7b. The maximum capture peak shifts downstream with increasing flow rate which is similar to the result with $Q<<Q_c$. However, a larger spreading is reported and is linearly dependent on the applied flow rate. The capture efficiency is also reported to be sensitive to the applied flow rate. Therefore, in this range of flow rate ($Q \approx Q_c$), the capture kinetics are not only controlled by the receptor-ligand interaction but also the flow rate (cell rolling speed).

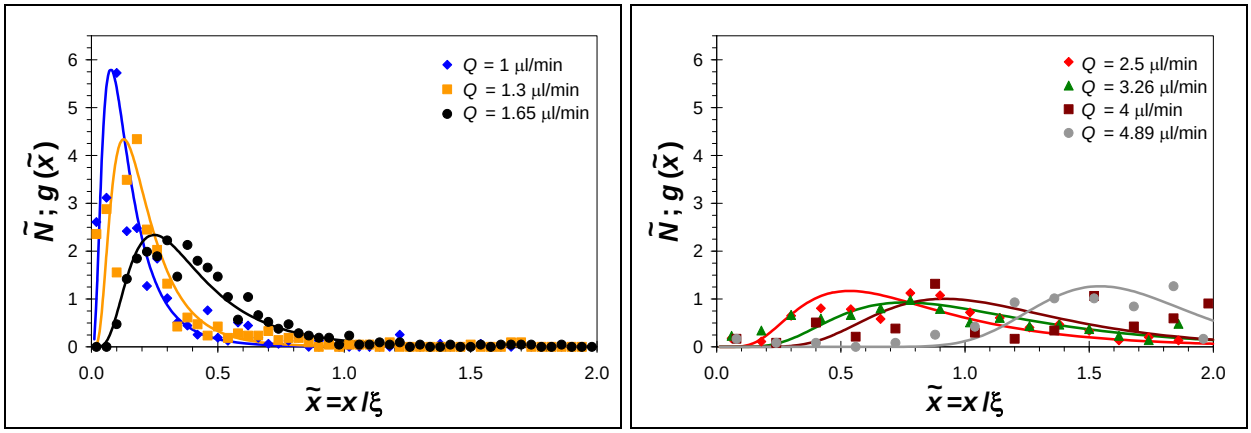

(a) (b)

Figure 7, Normalized spatial distribution of MDA-MB-231 cells captured in an EpCAM coated microchannel for: (a) $Q<Q_c$ and (b) $Q \sim Q_c$; log-normal distribution is fit to experimental data.

Under a high flow rate ($Q>>Q_c$), the cell is moving with very high speed such that the receptor and ligand do not have enough time to form a bond. In fact, even though a receptor-ligand complex is formed, the large hydrodynamic force will break the bond immediately and almost no cells are captured in the microchannel. Hence, the spatial distribution is not given. However, one can imagine that the spatial distribution is completely spread out to be zero everywhere due to the extremely large hydrodynamic force exerted on cell. In this range of flow rate ($Q>>Q_c$), the cancer cells are moving along with the flow field and the receptor-ligand interaction has almost no effect. Therefore, the kinetics is dominated by the hydrodynamic force that causes a cell to roll but not be captured in an antibody coated microchannel.

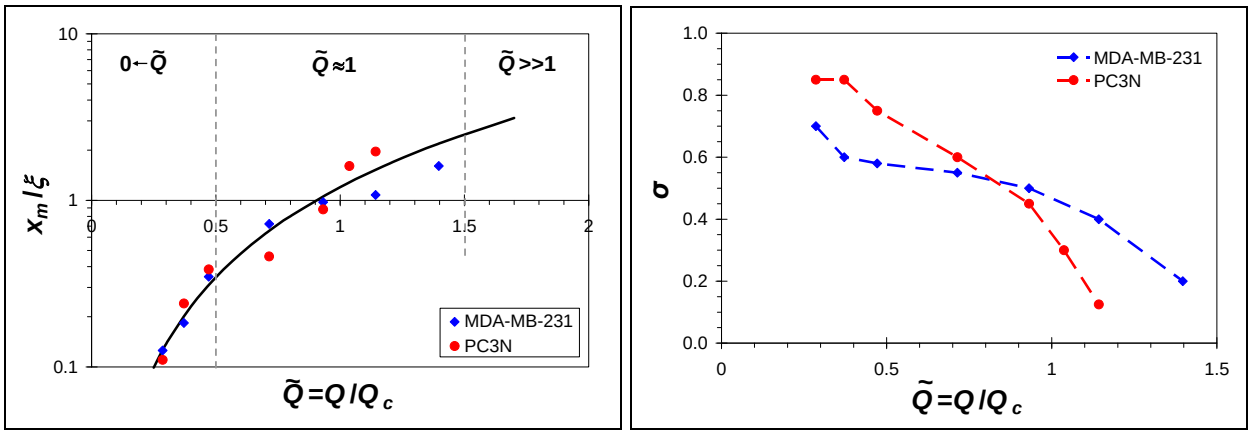

(a) (b)

Figure 8, Fitting parameters, (a) X_m/ξ and (b) σ, for the lognormal distribution.

From the statistical model, there are three zones classified by the comparison between Q and Q_c. To clearly identify these regions, the flow rate Q is normalized by Q_c as follows:

$$\tilde{Q} = Q / Q_c \tag{4}$$

When $Q<<Q_c$, the normalized flow rate $\tilde{Q} \to 0$ and the capture kinetics are similar to the no flow condition such that receptor-ligand interaction is the dominant mechanism. When $Q \approx Q_c$, the normalized flow rate $\tilde{Q} \approx 1$. It is in this transition region that both receptor-ligand interaction and cell rolling motion are comparable and important. When $Q>>Q_c$, the normalized flow rate $\tilde{Q} >> 1$, hydrodynamic force is dominant such that cells are rolling almost independently of the coating. The fitted μ value is the natural logarithm of the mean of x/ξ and the exponential function of μ is the median of the cumulative function which is defined as follows:

$$x_m / \xi = \exp(\mu) \tag{5}$$

The physical meaning of the median x_m is the distance to accumulate half of the total number of captured cells, $0.5 \times N_T$. The result is plotted against normalized flow rate $\tilde{Q}$ in Figure 8a. In the limit of $\tilde{Q} \to 0$, x_m/ξ is less than 0.5 such that half of the captured cells are located within a distance of 0.5ξ of the inlet. With further decreasing flow rates, the value x_m/ξ drops dramatically and seems to approach zero. For $\tilde{Q} \approx 1$, the normalized median increases with flow rate and the maximum value is about 2. Therefore, at least half of the total number of captured cells are attached within the first 2ξ of the microchannel for any given flow rate. This is a useful design criterion of an EpCAM coated microchannel to isolate target cancer cells from suspension. If the flow rate increases to $\tilde{Q} >> 1$, no cells are captured in the microchannel. The fitted standard deviation σ is plotted in Figure 8b. There is no clear distinct value discerning different regions. Actually, the σ value decreases monotonically with normalized flow rate. Two cell lines, PC3N and MDA-MB-231, have different rates of decay in σ which may be due to different numbers of receptors on the cell surfaces. The trend of σ agrees with the notion that the spatial distribution spreads out with increasing applied flow rate.

When the flow rate is small, the intrinsic rate constant k_{ad} for cell binding can be extracted from the spatial distribution. The first order kinetic attachment model has already been suggested for this purpose by other groups. However, this kinetic model is limited to relatively low flow rates. Here, our proposed log-normal distribution model overcomes this problem and can correctly describe the spatial cell pattern in a wide range of flow rates. To begin the k_{ad} calculation, the accumulation of captured cells (B) is defined as follows:

$$B(\tilde{x}) = \frac{1}{N_T} \int_0^{\tilde{x}} n(s) ds \tag{6}$$

where n is the number of captured cells in a particular location. To ensure that the receptor-ligand interaction dominates the kinetics, the intrinsic rate constant k_{ad} is estimated in the region of $\tilde{Q} \to 0$. Therefore, the experimental data corresponding to the lowest flow rate ($\tilde{Q}$ =0.28) are used in the calculation. Integrating g(x/ξ) yields the cumulative distribution function which is given as follows:

$$f(\tilde{x}; \mu, \sigma) = \frac{1}{2} + \frac{1}{2} erf\left[\frac{\ln \tilde{x} - \mu}{\sigma \sqrt{2}} \right] \tag{7}$$

Where μ equals -2.05 corresponding to x_m/ξ=0.129 and σ equals 0.9 in Figures 7a and 7b. These two statistical parameters are selected for the region of $\tilde{Q} \to 0$. To extract the intrinsic rate of binding from the cumulative curve, the expected value is calculated as follows:

$$E = \exp\left(\mu + \sigma^2 / 2\right) \tag{8}$$

The expected value is the average location for a capture event to occur, and the calculated E value is about 0.193. Referring to the measured cell rolling velocity, the intrinsic rate constant k_{ad} can be estimated as follows:

$$k_{ad} = \frac{U_{cell}}{E \cdot \xi} \tag{9}$$

The calculated k_{ad} is about 0.016 s^{-1}. To confirm this value, a separate calculation using the classical first order kinetics model reports almost the same k_{ad} value. Because the receptor-ligand interaction dominates the kinetics in the $\tilde{Q} \to 0$ region, the rate of binding k_{ad} is actually the summation of the association constant k_{on} and the unstressed dissociation constant k_{off}°. Using the k_{off}° of EpCAM reported in literature, 0.3×10^{-3} s^{-1}, the EpCAM association constant k_{on} is about 0.0157 s^{-1} in a functionalized microchannel. The reciprocal of k_{on} is about 1 min which represents the average time scale to form tight binding between a target cell and the immobilized EpCAM antibody. This value is consistent with the 1.5min time constant reported previously regarding cell capture in the static condition.

With increasing flow rate, higher force is exerted on the receptor-ligand binding causing dissociation. The force acting on the bond F_b can be calculated by using the mobility matrix model suggested by Korn *et al*. By comparing Goldman's solution with the measured cell rolling velocity, the gap distance between the cell and the microchannel surface is about 200nm and is used for mobility matrix calculations. From Bell's model, the dissociation constant k_{off} increases exponentially with the applied force as follows:

$$k_{off} = k_{off}^{\circ} \exp\left(x_\beta F_b / kT\right) \tag{10}$$

where x_β is the reactive compliance and equals 0.25nm, k is the Boltzmann constant and T is the absolute ambient temperature equal to 300K. The affinity constant $K_a=k_{on}/k_{off}$ is plotted against the normalized flow rate in Figure 9. Three zones corresponding to $\tilde{Q} \to 0$, $\tilde{Q} \approx 1$ and $\tilde{Q} >> 1$ are also indicated in the figure. The value of K_a is exponentially decreases from 50 to 0.01 with the given flow rate range. In one limit $\tilde{Q} \to 0$, the affinity constant K_a>10 such that $k_{on}>>k_{off}$. Once the receptor-ligand bond formed, the hydrodynamic force cannot break it. Therefore, almost all cells are captured in this limit of flow rate. In another limit $\tilde{Q} >> 1$, the affinity constant K_a<0.1 such that $k_{on}<<k_{off}$. Even though a receptor-ligand bond is formed, it cannot hold because the strong hydrodynamic force will break it. Consequently, the cell is purely rolling on the surface with no capture events occuring. In the transition $\tilde{Q} \approx 1$, the K_a is in between 0.1 to 10 such that k_{on} and k_{off} are comparable so there are no dominant kinetic mechanisms and the capture efficiency decreases with increasing applied flow rate. This transition zone can be further split into two sub-regions with $\tilde{Q} < 1$ and $\tilde{Q} > 1$. In the sub-region $\tilde{Q} < 1$, the K_a is larger than one and the resultant capture efficiency is higher than 50% as shown in Figure 6. On the other hand, the K_a is less than one if $\tilde{Q} > 1$ and the capture efficiency is reported to be less than 50%. Figure 9 provides a complete picture about the condition of cell capture in an antibody functionalized microchannel. It provides some useful design criteria for an antibody-based cell separation microdevice.

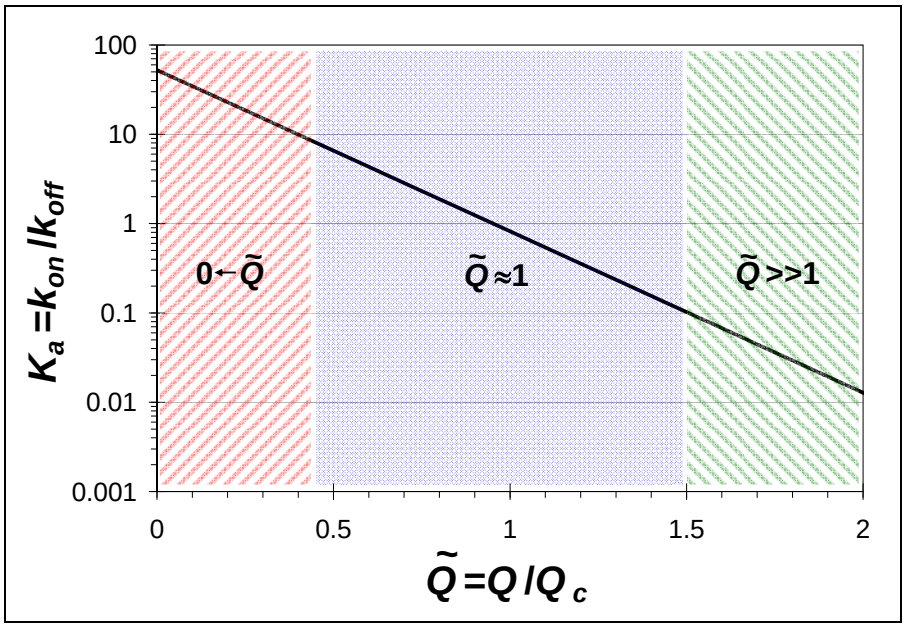

Figure 9, The affinity constant K_a is plotted against the normalized flow rate and three different colors represent $\tilde{Q} \to 0$, $\tilde{Q} \approx 1$ and $\tilde{Q} >> 1$ zones which have different dominant cell capture mechanisms.

III - Detachment of captured cancer cells under flow acceleration in a functionalized microchannel

Surfaces immobilized with antibodies are used to capture target cells from a suspension, and we have developed conditions to release the cells for further analysis. Cadherins make up a family of cell-cell adhesion molecules (receptors) and, in contrast with other trans-membrane receptors, adhesion of cadherins is homotypic; one cadherin subtype interacts only with an identical counter receptor. Therefore, since both PC3N and MDA-MB-231-N lines consist of cells with N-cadherin molecules, the microdevices are functionalized with N-cadherin antibodies for specific binding. Cell-attachment results indicate that a minimum of 5min incubation time is required to bind almost all PC3N or MDA-MB-231-N cells onto the antibody-functionalized channel surface. Since both the cell suspensions and the functionalized microchannels contain random experimental uncertainties, a conservative 15min incubation time has been selected for studying the response of captured cells subject to an applied shear flow. Once the binding between the cells and the functionalized surface is established, a certain level of fluid energy/flow rate is required to detach cells. However, the same flow rate Q can be obtained within different time intervals depending on the flow acceleration imposed by the pump setting. Here, flow acceleration is strictly defined as the flow rate increase with time, $dQ/dt>0$, different from convective acceleration that accounts for spatial gradients of the velocity field. Several flow acceleration levels have been tested and, for demonstration, only two cases corresponding to dQ/dt=0.33ml/min^2 (denoted as A) and 0.033ml/min^2 (denoted as B) are sketched in Figure 10. The tested flow conditions are represented by A_{jk} and B_{jk}; where the subscript j=1,2, …,n denotes the flow rate level, and k=1,2 denotes the start and finish of the following constant flow rate interval respectively. The HPLC pump is programmed to linearly increase the flow rate with time from zero to a desired level (solid lines connecting the origin with points A_{j1} & B_{j1}). Once the design flow rate is achieved, the pump maintains the flow rate constant for additional 5min to obtain a steady state (dash lines connecting points A_{j1} & B_{j1} with A_{j2} & B_{j2}). At the end of the constant flow rate interval, the pump shuts down stopping the flow.

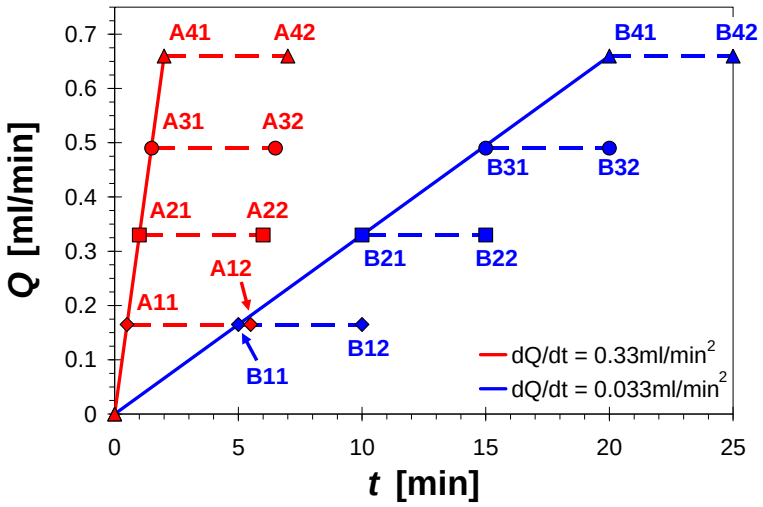

Figure 10, A summary of two example experimental conditions, high (red) and low (blue) flow acceleration, under which cell detachment has been examined; symbols represent instances at which either the flow acceleration (A_{j1} & B_{j1}) or the flow rate is switched off (A_{j2} & B_{j2}).

As the flow accelerates, an attached cell experiences hydrodynamic loads (force and moment) increasing with time and, in response, the cell is deformed. To demonstrate the effect of flow acceleration on cell deformation, video clips of captured PC3N cells under accelerating flow rates have been recorded. Using a Matlab image processing program, the cell projected area A is measured from the recorded images. The cell area, normalized by its initial area under zero flow rate A_0, is plotted in Figure 11 as a function of the instantaneous flow rate for both flow accelerations. Under low acceleration, the cell projected area initially increases almost linearly with flow rate, up by about 30% at Q=0.25ml/min. Then, the deformation rate is slowly leveled off approaching a larger projected area by about 40% at Q=0.4ml/min. In comparison, under high acceleration, the cell retains its projected circular area. Increasing the flow rate further, Q>0.5ml/min, results in detachment of almost all the captured cells.

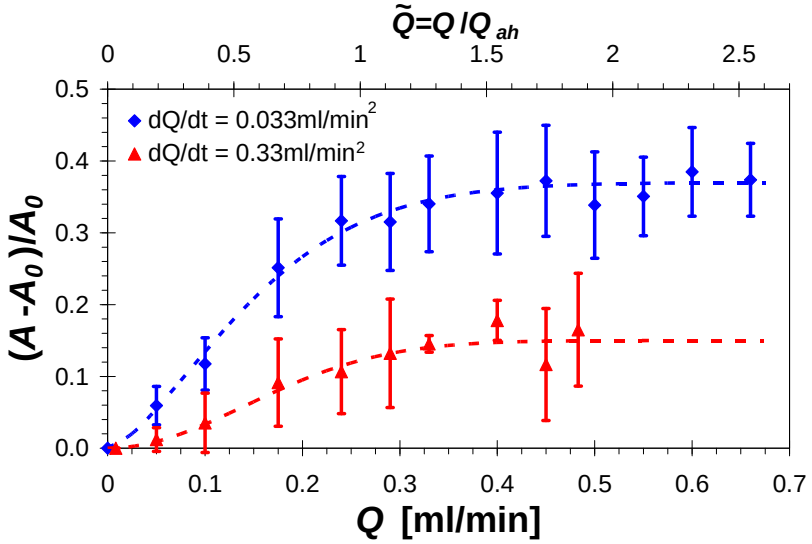

Figure 11, The dependence of the cell projected area (top view), normalized by its initial area, on the instantaneous flow rate for both low and high acceleration.

The dramatic difference in cell deformation under the same flow rate due to varying flow acceleration is consistent with the well-documented viscoelastic behavior of biological cells. A homogeneous standard linear solid (SLS) model has been proposed to describe cell response to external mechanical loading. The model contains a damping element controlling the deformation rate, and a damping mechanism explicitly implies that a cell requires a finite time to deform in response to mechanical loads. Therefore, when a mechanical load is applied within a short period of time, as in high acceleration, the cell cannot respond simply retaining its original shape similar to a solid object. On the other hand, under low acceleration when the loading is slowly ramped up, the cell has enough time to completely deform as a compliant material in a quasi-steady manner. Although the cell viscoelastic property has previously been associated with micropipette aspiration and mechanical indentation, the present results verify this behavior in cell response to hydrodynamic loading as well. Hence, flow acceleration should be a critical control parameter in determining the captured-cell response to fluid flow in a microchannel.

Assuming the cell volume is conserved during the relatively short flow-acceleration experiments (less than 30min); increased projection area due to hydrodynamic loading necessarily entails a decrease in the cell height. Following a proposed geometric model for a captured cell subject to shear flow, the height of a tear-shaped cell is about half the height of the original hemispherical cell under no flow. The lower cell profile in turn results in reduced hydrodynamic loads. Thus, under lower flow acceleration, captured cells experience lower hydrodynamic loads when exposed to the same flow rate. Consequently, even assuming constant cell-surface binding force, higher flow rate will be required to detach such highly-deformed cells. Furthermore, the cell adhesion force to the antibody-functionalized surface may not stay constant. It is plausible to assume that the number of binding sites is approximately proportional to the cell contact area; and, since a cell projected area under lower acceleration is larger, the cell adhesion force might also be larger. Consequently, a higher flow rate would be required to detach a captured cell subject to lower flow acceleration due to both lower profile, leading to lower hydrodynamic loading, and larger contact area, resulting in higher binding force.

Detachment of PC3N cells bound to an anti-N-cadherin functionalized surface due to applied shear flow in a microchannel has been investigated focusing on the effect of flow acceleration. To this end, different flow acceleration levels have been tested including a ‘step function’ case, in which the flow rate is increased as fast as the mechanical pump allows (dQ/dt=4.5ml/min^2). In each test, the prepared PC3N cell suspension is loaded into a functionalized microchannel, followed by 15min incubation time. After washing, the number of captured cells N_0 is counted and, usually, it is equal to the number of initially loaded cells N_i. Next, the flow rate increases linearly with time (dQ/dt=const) from zero until a prescribed flow rate Q is obtained; several flow rates have been selected for each of the tested flow acceleration. This is followed by a 5min interval of constant flow rate, i.e. dQ/dt=0, to establish steady-state conditions. The pump is then turned off, at the end of the constant flow rate stage, and the number of the remaining captured cells N_a is counted. The number of detached cells, $N=N_0-N_a$, normalized by the initial number of captured cells, N_0, is plotted in Figure 12a as a function of the normalized prescribed flow rate for all tested flow accelerations; the flow rate required for removing half of the captured cells under ‘step function’ flow acceleration, Q_{ah}=0.26ml/min, is chosen for flow rate scaling.

All curves start at the origin as no cell can be detached under no flow condition (Q=0). With increasing flow rate, the fraction of detached cells increases gradually towards unity indicating complete removal of all initially captured cells. If all captured cells are identical, i.e. having the same number of binding sites with the same bond strength, then all cells should be detached at the lowest flow rate above which the hydrodynamic loads overcome the adhesion forces. However, the cells vary among themselves in size and membrane properties, while the antibody-coated surfaces and the applied shear flows are not perfectly uniform as well. Consequently, the cell-surface binding force is randomly distributed within a certain range, requiring different flow rates to detach various captured cells as has been observed. However, if only the flow rate level is relevant in determining the hydrodynamic loads on a captured cell, all the results in Figure 12a should collapse into a single curve regardless of flow acceleration. It is clearly not the case as the fraction of detached cells monotonically increases with increasing flow acceleration under the same flow rate; e.g., at $Q=2Q_{ah}$, the fraction of detached cells increases from about 0.4 under 0.016ml/min^2 to about 0.95 under 0.81ml/min^2 acceleration. This indicates that flow acceleration affects both the hydrodynamic loads and the adhesion forces experienced by a captured cell under a certain flow rate consistent with the cell deformation results. An interesting feature of the data shown in Figure 12a is the apparent lower bound on the flow acceleration, below which the effect of flow acceleration vanishes; the curves corresponding to dQ/dt=0.033ml/min^2 and 0.016ml/min^2 are the same within experimental error. This lower bound limit represents a 'quasi-steady' cell behavior, in which the cell has sufficient time to fully respond to the instantaneous flow field as in a steady-state flow. Lowering further the flow acceleration rate, dQ/dt<0.016ml/min^2, will result in a similar response depending only on the flow rate. On the other hand, the 'step function' acceleration represents an upper bound limit. Since the cell has no time to respond, its detachment must depend only on the instantaneous flow rate. Indeed, increasing the flow acceleration level from dQ/dt=0.81ml/min^2 to 4.5ml/min^2 results in the same cell detachment rate.

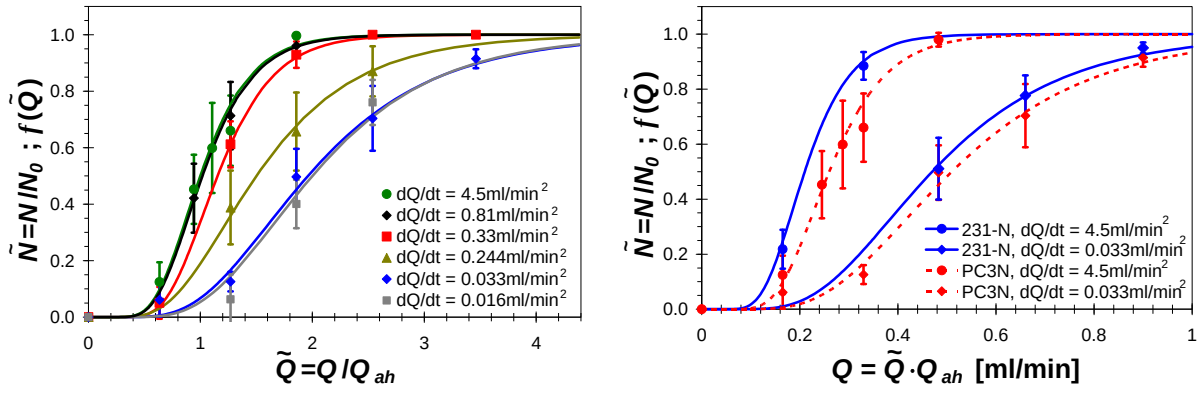

(a) (b)

Figure 12, (a) A comparison between the measured fraction of detached PC3N cells as a function of the applied flow rate (symbols) and fitted log-normal probability distribution functions calculated based on Equation 11 (curves) for various flow accelerations; and (b) a comparison between the limiting flow accelerations, 'step function' and 'quasi steady', for the PC3N and the MDA-MB-231-N cells.

The effect of flow acceleration on detachment of MDA-MB-231-N cells, bound to an anti-N-cadherin functionalized surface, has also been investigated. Similar behavior has been observed and, for clarity, only the fraction of detached cells under the upper and lower flow acceleration

bounds are compared in Figure 12b with the corresponding PC3N results. The only difference between the two sets of data is the slight shift of the MDA-MB-231-N results to the left; namely, to detach the same fraction of captured cells, MDA-MB-231-N cells require lower flow rate than PC3N cells. This may indicate that the binding of the smaller MDA-MB-231-N cells (D~15μm) is weaker than the binding of the larger PC3N cells (D~20μm). If so, the apparent weaker binding of MDA-MB-231-N cells could perhaps be due to a smaller cell-surface contact area.

Each curve in Figures 12a and b represents a cumulative distribution function bound between 0 and 1. The varying flow rate required for cell detachment can be thought of as a product of several independent and random factors, e.g. binding forces and hydrodynamic loads. Hence, the cell-detachment flow rate can statistically be modeled as log-normal, and the following probability distribution function f is fitted to each flow acceleration data set:

$$f(\tilde{Q};\mu,\sigma) = \frac{1}{2} + \frac{1}{2}\,\mathrm{erf}\left[\frac{\ln\tilde{Q} - \mu}{\sigma\sqrt{2}}\right] \tag{11}$$

with μ and σ, the mean and standard deviation of the flow-rate natural logarithm, being the fitting parameters. The normalized variables and the mean distribution are defined as:

$$\tilde{N} = \frac{N}{N_0} \;\; ; \;\; \tilde{Q} = \frac{Q}{Q_{ah}} \;\; ; \;\; \mu = \ln\left(\frac{Q_a}{Q_{ah}}\right) \tag{12}$$

For convenience, Q_a is selected as the flow rate required for detachment of half of the captured cells; thus, the standard deviation is the only free parameter adjusted to obtain the best fit of Equation 11 depending on the flow acceleration. The pairs of fitting parameters, Q_a/Q_{ah} and σ, determined for PC3N cells under all tested flow accelerations are listed in Table 1.

Table 1: The parameters used to fit the log-normal cumulative distribution functions to the measured fraction of detached PC3N cells for various flow accelerations

	Flow acceleration, dQ/dt					
	0.016ml/min^2	0.033ml/min^2	0.244ml/min^2	0.33ml/min^2	0.81ml/min^2	4.5ml/min^2
$\boldsymbol{Q_a}$ [ml/min]	0.52 (Q_{as})	0.51	0.39	0.30	0.265	0.26 (Q_{ah})
$\boldsymbol{\sigma}$	0.43	0.45	0.46	0.34	0.35	0.35
$\boldsymbol{\theta}$ [min]	16.25	7.879	1.066	0.788	0.321	0.058

The agreement between the fitted probability distribution functions and the measured experimental results in Figures 12a and b indicates both: the suitability of the log-normal statistical model to analyze the cell detachment results, and the proper selection of the scaling parameters. Therefore, though difficult to confirm experimentally, it should be interesting to examine the complimentary probability density function g for a log-normal distribution; it is readily available by differentiating the probability density function in Equation 11, with respect to the normalized flow rate, as follows:

$$g(\tilde{Q};\mu,\sigma) = \frac{\mathrm{d}f}{\mathrm{d}\tilde{Q}} = \frac{1}{\tilde{Q}\sigma\sqrt{2\pi}}\exp\left[-\frac{(\ln\tilde{Q} - \mu)^2}{2\sigma^2}\right] \tag{13}$$

The resulting curves, based on Equation 13, are plotted in Figures 13a and b for each acceleration flow depicted in Figures 12a,b. As the flow acceleration decreases, for the two cell types PC3N and MDA-MB-231-N, the peak shifts to a higher flow rate with a wider distribution; i.e. both μ and σ decrease with increasing dQ/dt. Log-normal distributions have also been

observed in measurements of strength of bonds between biological receptor molecules and their ligands, as well as in measurements of forces required for rapid detachment of agglutinin-bonded red blood cells. These results led to the notion that the number of binding sites of a captured cell is a discrete, time-dependent, random variable with significant fluctuations; thus, a probabilistic theory has been applied to describe the state of such systems. Consistent with the distributions depicted in Figures 13a and b, both the rupture force and its standard deviation are reported to increase with increasing number of bonds or force loading rate.

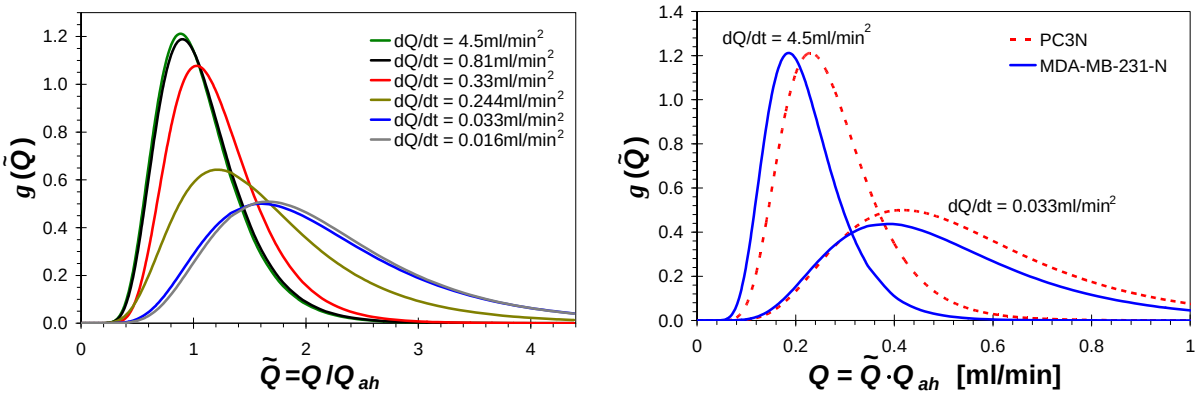

(a) (b)

Figure 13, (a) Log-normal probability density functions of PC3N cells detached from an anti-N-cadherin functionalized microchannel calculated based on Equation 13 for the probability distribution functions plotted in Figure 12a, and (b) probability density functions for captured PC3N and MDA-MB-231-N cell subject to the 'step function' and 'quasi steady' accelerations corresponding to Figure 12b.

The cell detachment results indicate that, under the same flow rate, the fraction of detached cells strongly depends on the loading rate (flow acceleration). This can be viewed as a balance between two competing time scales; a detachment-force time scale determined by the externally-applied flow acceleration and a cell-deformation time scale depending on the inherent cell physiology. The characteristic time scale for the hydrodynamic loading depends on the applied accelerating flow, dQ/dt, and it is normalized by the characteristic flow rate Q_{ah} to obtain the correct dimensions of time as follows:

$$\theta = \left(\frac{1}{Q_{ah}} \frac{\mathrm{d}Q}{\mathrm{d}t} \right)^{-1} \tag{14}$$

This scaling represents the ramping-up time needed for the flow rate to reach the required level of Q=Q_{ah} under various flow accelerations as listed in Table 1; these data can now be used to estimate the time scale for the cell mechanical response. The fitted standard deviation for PC3N is plotted in Figure 14 as a function of the normalized flow acceleration. The results are grouped around two levels, 0.35 for relatively high and 0.45 for low flow acceleration, with a sharp jump between them. The lower standard deviation at high acceleration is mainly due to the initial randomness of the cell-surface binding force after incubation. However, due to the cell deformation under low flow acceleration, the randomness in the cell-surface binding forces increases with increasing cell projected area. Similarly, in a molecular study of a receptor-ligand binding force, both the rupture force and its standard deviation are found to increase with increasing number of binding sites. Recalling the results plotted in Figure 11, a deformed cell under low acceleration has a larger projected area and potentially larger number of binding sites

in comparison to a cell under high flow acceleration. Therefore, the time corresponding to the jump in the standard deviation level, τ=1.15min, can be considered as the proper time scale characterizing the PC3N cell mechanical response to hydrodynamic loading. The characteristic time scale for MDA-MB-231-N cells is lower, τ=0.85min.

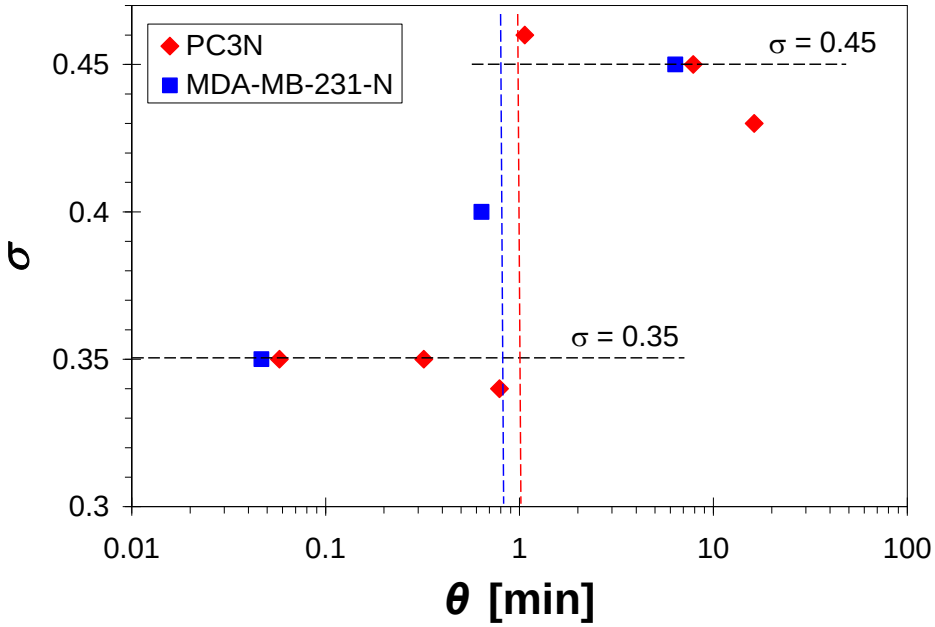

Figure 14, The dependence of the distribution standard deviation (σ) on the flow acceleration (dQ/dt) normalized by the characteristic flow rate (Q_{ah}) showing a jump around a characteristic time scale of τ= 1.15 and 0.85min for the PC3N and MDA-MB-231-N cells, respectively.

The flow rate required for cell detachment has been analyzed in previous studies as a function of the specific cell-surface system only; however, the present results suggest that it also depends on flow acceleration. The explicit dependence of the flow rate required for detaching half of the captured cells, Q_a, on the flow acceleration, dQ/dt, should therefore be explored to quantify this effect. Two limits have been discovered in the cell detachment experiments: 'step function' acceleration, providing a lower limit Q_a=Q_{ah}, and 'quasi steady' acceleration, providing an upper limit Q_a=Q_{as}; hence, proper scaling of Q_a should involve both limiting parameters Q_{ah} and Q_{as}. Furthermore, the cell mechanical time scale τ is utilized to render the flow acceleration dimensionless. Using these scaling arguments, the normalized flow rate required for detachment of the two cell types, PC3N and MDA-MB-231-N, is plotted in Figure 15 as a function of the normalized flow acceleration. A simple mathematical model describing a sharp transition between two asymptotic levels is the following exponential function:

$$\hat{Q}_a = \frac{Q_a - Q_{ah}}{Q_{as} - Q_{ah}} = 1 - \exp\left(-\hat{t}^{\,b}\right) \quad ; \quad \hat{t} = \theta / \tau \tag{15}$$

In this scaling, the normalized required flow rate is conveniently bound between 0 and 1 with the normalized time for the sharp transition around 1, and the only fitting parameter is the exponent b. The results for both cell types not only collapse onto a single curve but also, with b=4, the agreement between the calculations and measurements is remarkable. Therefore, the reported cell detachments behavior is not limited to a particular cell type but can be extended to other

cell-surface combinations. Furthermore, the empirical formula describes properly the transition from high to low flow acceleration regime characterizing the mechanical detachment of captured cells due to hydrodynamic loading.

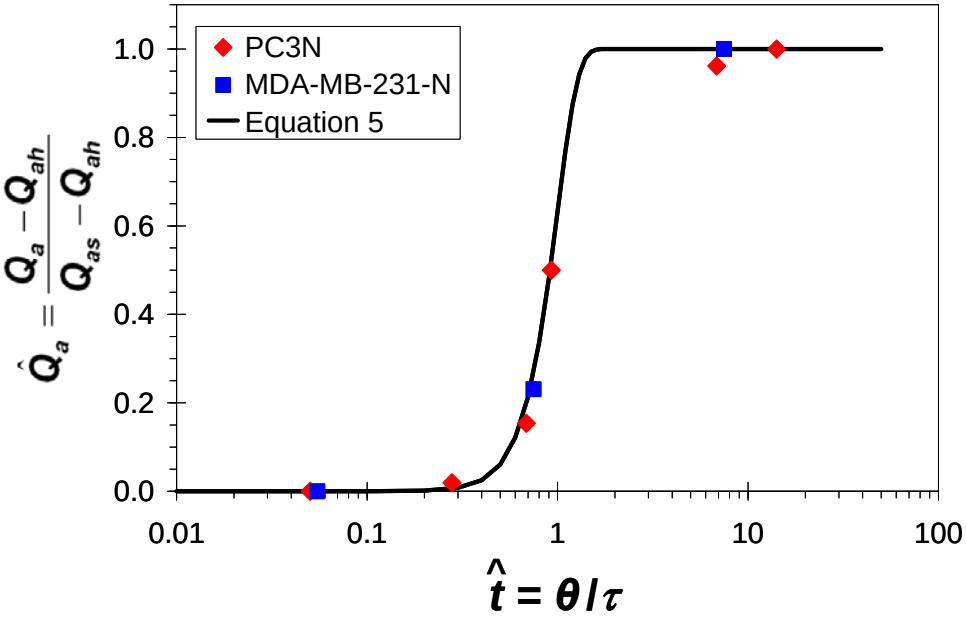

Figure 15, A comparison between the normalized flow rate required for detachment of half of the captured cells Q_a measured as a function of the normalized flow acceleration θ (symbols), for both PC3N and MDA-MB-231-N cells, and the empirical exponential formula in Eqn. 5 fitted with b=4 (solid line).

The SLS model has originally been proposed to study small-strain deformation of living cells undergoing micropipette aspiration. The whole cell is modeled as a homogeneous linear viscoelastic solid with two elastic, k_1 and k_2, and one viscous element, η, represented by two springs and a dashpot; the characteristic time response of such a system is given by $\eta(k_1+k_2)/(k_1k_2)$. Spring and damping constants have been measured for a variety of cells under different conditions, yielding a time constant in the range of 0.5-2min. Indeed, the estimated response time of a captured PC3N or MDA-MB-231-N cell to applied hydrodynamic loading, 1.15 and 0.85min respectively, is well within this range. The effect of flow acceleration can now be summarized as follows: under high acceleration, $\theta<\tau$, the cell deformation is negligible resulting in high hydrodynamic loads; consequently, low flow rate is sufficient for cell detachment as $Q_a \rightarrow Q_{ah}$; under low acceleration, $\theta>\tau$, the cell deformation is significant resulting in both low hydrodynamic loads and possibly higher binding forces; thus, high flow rate is needed for cell detachment as $Q_a \rightarrow Q_{as}$. It is important to note that Q_{ah}, Q_{as} and τ are characteristics of a particular system including cell type, surface coating, buffer solution and microchannel geometry. Varying any of these parameters will necessarily lead to a different set of values. Furthermore, similar to either the average velocity or the wall shear stress, the flow rate is only a representative of the hydrodynamic loading. The actual loads depend on the detailed stress distribution around the cell membrane; obtaining this stress field requires a major effort yet to be conducted. Finally, only the mechanical response of captured cells to applied hydrodynamics loads has been analyzed. The biochemical response including the viability of detached cells, though critical in many applications, is outside the scope of this work.

Key Research Accomplishments

- High-specificity capture of cancer cells in antibody-functionalized microchambers:
    - Specific capture of cells from suspensions increases exponentially with incubation time and linearly with concentration, for dilute suspensions, with almost 100% capture efficiency.
    - Poor capture is obtained, less than 10%, when changing cell type with different membrane receptors, changing the ligands immobilized on the surface, or incubating the cell suspension at low temperature.

- Capture of cancer cells in antibody-functionalized microchannels (1000μm wide and 100μm deep) under shear flow:
    - A critical flow rate, about Q_c=3.5μl/min, has been identified,
        - At $Q<Q_c$, receptor-ligand interaction dominates; almost all cells are captured.
        - At $Q>Q_c$, hydrodynamic loading dominates such that no cell is captured.
        - At $Q\approx Q_c$, the capture efficiency decreases rapidly with increasing flow rate.
    - The spatial distribution of captured cells follows a log-normal statistics,
        - At lower flow rate, $Q<Q_c$, a sharp peak close to the channel inlet with a relatively small spatial spread is observed.
        - At intermediate flow rate, $Q\approx Q_c$, the peak location shifts downstream with a larger spatial spread.
    - The flow rate effect on the cell capture kinematics is a result of the ratio between the binding association/dissociation rate constants.

- Captured cancer cells on functionalized surfaces have successfully been detached, and the required flow rate for detachment is random described by a log-normal distribution:
    - Two flow acceleration limits have been identified,
        - 'Step function' acceleration, with negligible cell deformation, requiring low flow rate for cell detachment.
        - 'Quasi-steady' acceleration, with significant cell deformation, requiring high flow rate for cell detachment.
    - A time constant of about 1min, consistent with the cell viscoelastic nature, characterizes the mechanical response of a captured cell to hydrodynamic loading.
    - A unified empirical exponential function is found to predict the flow rate required for cell detachment as a function of flow acceleration for both cancer cell types.
    - The detached cells are found to be viable.

Reportable Outcomes

- Cheung, L.S.L., Zheng, X.J., Stopa, A., Schroeder, J.A., Heimark, R.L., Baygents, J.C., Guzman, R. & Zohar, Y. 2009 Detachment of captured cancer cells under flow acceleration in a bio-functionalized microchannel. *Lab-on-a-Chip*, **9**, 1721-1731.
- Zheng, X.J., Cheung, L.S.L., Wang, L., Schroeder, J.A., Heimark, R.L., Baygents, J.C., Guzman, R. & Zohar, Y. 2009 Specific binding of cancer cells using a micro chamber functionalized with antibodies. Submitted to the *2009 ASME International Mechanical Engineering Congress & Exposition,* Lake Buena Vista, FL, November 13-19, 2009.

Conclusions

Microchambers have been fabricated in silicon wafers, using a DRIE process, and functionalized with bio-active layers. Several parameters affecting the specificity of cell binding to the functionalized surfaces have been investigated. Specific capture of cancer cells from suspensions increases exponentially with incubation time and linearly with concentration. Functionalizing a surface with specific counter-receptors enables capture of almost 100% of cells with matching receptors within 15min incubation time at ambient temperature higher than 25°C. Suspending cells with different receptors, changing the counter receptors immobilized on the surface, or incubation the cell suspension at low ambient temperature result in a poor capture rate.

A microchannel functionalized by EpCAM or N-cadherin antibodies has been utilized to study the behavior of a homogeneous suspension of PC3N prostate and MDA-MB-231 breast cancer cells subject to hydrodynamic loading. With increasing the flow rate Q, the capture efficiency decays exponentially and the control parameter Q_c is reported to be 3.5μl/min. In one limit, $Q<<Q_c$, the effect of receptor-ligand interaction dominates due to the cell slow movement. Therefore, almost all the cells are captured in this flow rate. In the other limit, $Q>>Q_c$, the fluid motion overcomes the interaction time between receptor and ligand such that none of the rolling cells is captured. A transition region, $Q\approx Q_c$, intermediates the two asymptotic limits where both fluid motion and receptor-ligand interaction are important. In this range, the capture efficiency drops rapidly with increasing flow rate. The flow rate also affects the captured cell spatial distribution. A sharp maximum peak and narrow spreading is observed if $Q<<Q_c$. On the other hand, a significant large spreading is found when $Q\approx Q_c$ indicating the transition state. Further increase in the flow rate, $Q>Q_c$, the maximum peak shifts to the channel outlet and no cell is captured within the finite-length channel. This result suggests that the competition between receptor-ligand association/dissociation rate (k_{on} or k_{off}) and the hydrodynamic motion (Q) time scale determines the kinematic details of cell capture in a bio-functionalized microchannel.

A microchannel functionalized by N-cadherin antibodies has been utilized to study the behavior of a homogeneous suspension of N-cadherin expressing PC3N prostate and MDA-MB-231-N breast cancer cells subject to hydrodynamic loading. Following 15min incubation time to ensure steady-state cell-surface interaction, the effect of flow acceleration has been investigated. A captured cell maintains its spherical shape with little deformation under high, while it is significantly deformed attaining a tear-drop shape under low flow acceleration. The required flow rate for cell detachment is random in nature, and is adequately described by a log-normal distribution. Two flow acceleration limits have been identified corresponding to: (i) ‘step function’ acceleration requiring the minimum flow rate for cell detachment with a small standard deviation, and (ii) ‘quasi-steady’ acceleration requiring the maximum flow rate for cell detachment with a large standard distribution. The sharp transition from the low to high standard deviation provides a time constant of about 1min for the mechanical response of a captured cancer cell to hydrodynamic loading. Utilizing both detachment flow rate limits and the cell mechanical time constant, a unified empirical exponential function is found to predict the flow rate required for cell detachment as a function of flow acceleration for both cancer cell types.

References

R. Alon, D. A. Hammer and T. A. Springer, Lifetime of the P-selectin-carbonhydrate bond and its response to tensile force in hydrodynamic flow, *Nature*, 1995, **374**, 539-542.

M. Balzar, M. J. Winter, C. J. de Boer, S. V. Litvinov, The biology of the 17-1A antigen (Ep-CAM), *J. Mol. Med.*, 1999, **77**, 699-712.

J. Cao, B. Donel, Daniel R. Deaver, M. B. Lawrence and C. Dong, In vitro side-view imaging technique and analysis of human T-leukemic cell adhesion to ICAM-1 in shear flow, *Microvasc. Rec.*, 1998, **55**, 124-137.

W. C. Chang, L. P. Lee and D. Liepmann, Biomimetic technique for adhesion-based collection and separation of cells in a microfluidic channel. *Lab Chip*, 2005, **5**, 64-73.

X. Cheng, D. Irimia, M. Dixon, K. Sekine, U. Demirci, L. Zamir, R. G. Tompkins, W. Rodriguez and M. Toner. A microfluidic device for practical label-free CD4+ T cell counting of HIV-infected subjects. *Lab Chip*, 2007, **7**, 170-178.

L. Cheng, X. Xia, W. Yu, L. E. Scriven and W. W. Gerberich, Flat-punch indentation of viscoelastic material, *J. Polymer Sci.*, 2000, **38**, 10-22.

L. S. L. Cheung, X. J. Zheng, A. Stopa, J. Schroeder, R. L. Heimark, J. C. Baygents, R. Guzman and Y. Zohar, Attachment & detachment of prostate cancer cells in a microfluidic system, Proceedings of the 12th International Conference on Miniaturized Systems for Chemical and Life Sciences, San Diego, USA, 2008, 1159-1161.

L. S. L. Cheung, X. J. Zheng, A. Stopa, J. Schroeder, R. L. Heimark, J. C. Baygents, R. Guzman and Y. Zohar, Flow acceleration effect on cancer cell deformation and detachment, Proceedings of the 22nd IEEE International Conference on Micro Electro Mechanical Systems, Sorrento, Italy, 2009, 431-434.

M. Cristofanilli, G. T. Budd, M. J. Ellis, A. Stopeck, J. Matera, M. C. Miller, J. M. Reuben, G. V. Doyle, W. J. Allard, L. W.M.M. Terstappen and D. F. Hayes, Circulating tumor cells, disease progression, and survival in metastatic breast cancer, *N. Engl. J. Med.*, 2004, **351**, 781-791.

Z. Du, K. H. Cheng, M. W. Vaughn, N. L. Collie and L. S. Gollahon, Recognition and capture of breast cancer cells using a antibody-based platform in a microelectromechanical systems device, *Biomed. Microdevices*, 2007, **9**, 35-42.

E. Evans, D. Berk and A. Leung, Detachment of agglutinin-bonded red blood cells, *Biophys. J.*, 1991, **59**, 838-848.

R. Iwama, L.M. Lee, E.S. Cho, and Y. Zohar, "Fabrication of microchannels with patterned bio-active layers," *Proc. MEMS2007*, pp. 333-336, 2007.

A. Jemal, R Siegel, E. Ward, Y. Hao, J. Xu, T. Murray and M. J. Thun, Cancer statistics 2008, *CA Cancer J. Clin.*, 2008, **58**, 71-96.

H. J. Kahn, A. Presta, L-Y. Yang, J. Blondal, M. Trudeau, L. Lickley, C. Holloway, D. R. McCready, D. Maclean and A. Marks, Enumeration of circulating tumor cells in the blood of breast cancer patients after filtration enrichment: correlation with disease stage, *Breast Cancer Res. Treast.*, 2004, **86**, 237-247.

E. J. Koay, A. C. Shieh and K. A. Athanasiou, Creep indentation of single cells, *J. Biomech. Eng.*, 2003, **125**, 334-341.

D. Leckband and A. Prakasam, Mechanism and dynamics of cadherin adhesion, *Annu. Rev. Biomed. Eng.*, 2006, **8**, 259-287.

L. M. Lee, R. L. Heimark, J. C. Baygents and Y. Zohar, Self-aligned immobilization of proteins utilizing PEG patterns, *Nanotechnology*, 2006, **17**, S29-S33.

L. M. lee, R. L. Heimark, R. Guzman, J. C. Baygents and Y. Zohar, Low melting point agarose as a protection layer in photolithographic patterning of aligned binary proteins, *Lab Chip*, 2006, **6**, 1080-1085.

C. T. Lim, E. H. Zhou and S. T. Quek, Mechanical models for living cells–a review, *J. Biomech.*, 2006, **39**, 195-216.

R. Merkel, P. Nassoy, A. Leung, K. Ritchie and E. Evans, Energy landscapes of receptor-ligand bonds explored with dynamic force spectroscopy, *Nature*, 1999, **397**, 50-53.

J.G. Mohanty, J.S. Jaffe, E.S. Schulman, D.G. Raible, A highly sensitive fluorescent micro-assay of H2O2 release from activated human leukocytes using a dihydroxyphanoxazine derivative", *J. Immunol Methods*, vol. 202, pp133-141 ,1997.

S. Nagrath, L. V. Sequist, S. Maheswaran, D. W. Bell, D. Irimia, L. Ulkus, M. R. Smith, E. L. Kwak, S. Digumarthy, A. Muzikansky, P. Ryan, U. J. Balis, R. G. Tompkins, D. A. Haber and M. Toner, Isolation of rare circulating tumor cells in cancer patients by microchip technology, *Nature*, 2007, **450**, 1235-1239.

P. Panorchan, M. S. Thompson, K. J. Davis, Y. Tseng, K. Konstantopoulos and D. Wirtz, Single-molecule analysis of cadherin-mediated cell-cell adhesion, *J. Cell Sci.*, 2006, **119**, 66-74.

T. Park, T. Jensen, D. Park, J. Guy, P. Datta, S.A. Soper, and M.C. Murphy, "Capture of very rare circulating tumor cells for human breast cancer diagnosis," *Proc. IMECE2007*, IMECE2007-42425, 2007.

B. D. Plouffe, M. Radisic and S. K. Murthy, Microfluidic depletion of endothelial cells, smooth muscle cells, and fibroblasts from heterogeneous suspensions. *Lab Chip*, 2008, **8**, 462-472.

M. Sato, N. Ohshima and R. M. Nerem, Viscoelastic properties of cultured porcine aortic endothelial cells exposed to shear stress, *J. Biomech.*, 1996, **29**(4), 461-467.

M. Sato, D. P. Theret, L. T. Wheeler, N. Ohshima and R. M. Nerem, Application of the micropipette technique to the measurement of cultured porcine aortic endothelial cell viscoleastic properties, *J. Biomech. Eng.*, 1990, **112**, 263-268.

G. W. Schmid-Schönbein, K-L. P. Sung, H. Tōzeren, R. Skalak and S. Chien, Passive mechanical properties of human leykocytes, *Biophys. J.*, 1981, **36**, 243-256.

S. F. Sener, B. Cady and D. Merkel, Primary factor in declining breast cancer mortality rates – Early detection or adjuvant therapy?, *Cancer Pract.*, 2002, **10**(1), 45-47.

M. S. Simon, D. Ibrahim, L. Newman and M. Stano, Efficacy and economics of hormonal therapies for advanced breast cancer, *Drugs Aging*, 2002, **19**(6), 453-463.

J. B. Smerage and D. F. Hayes, The measurement and therapeutic implications of circulating tumor cells in breast cancer, *Br. J. Cancer*, 2006, **94**, 8-12.

D. P. Theret, M. J. Levesque, M. Sato, R. M. Nerem and L. T. Wheeler, The application of a homogeneous half-space model in the analysis of endothelial cell micropipette measurements, *J. Biomech. Eng.*, 1988, **110**, 190-199.

M. Toner, and D. Irimia, "Blood-on-a-chip," *Annu. Rev. Biomed. Eng.*, vol. 7, pp. 77-103, 2005.

V. Towne, M. Will, B. Oswald, Q. Zhao, "Complexities in horseradish peroxidase-catalyzed oxidation of dihydroxyphanoxazine derivatives: appropriate ranges fro pH values and hydrogen peroxide concentrations in quantitative analysis," *Analytical Biochemistry*, vol. 334 pp. 290-296, 2004.

N. L. Tran, R. B. Nagle, A. E. Cress and R. L. Heimark, N-Cadherin expression in human prostate carcinoma cell lines: An epithelial-mesenchymal transformation mediating adhesion with stromal cells. *AJP*, 1999, **155**(3), 787-798.

P. T. Went, A. Lugli, S. Meier, M. Bundi, M. Mirlacher, G. Sauter and S. Dirnhofer, Frequent EpCam protein expression in human carcinomas, *Hum. Pathol.*, 2004, **35**, 122-128.

F. Wärnberg, H. Nordgren, L. Bergkvist and L. Holmberg, Tumour markers in breast carcinoma correlate with grade rather than with invasiveness, *Br. J. Cancer*, 2001, **85**(6), 869-874.

B. P. L. Wijnhoven, W. N. M. Dinjens and M. Pignatelli, E-cadherin-catenin cell-cell adhesion complex and human cancer, *BJS*, 2000, **87**, 992-1005.

X. Zhang, P. Jones and S. J. Haswell, Attachment and detachment of living cells on modified microchannel surfaces in a microfluidic-based lab-on-a-chip system, *Chem. Eng. J.*, 2008, **135S**, S82-S88.

C. Zhu, G. Bao and N. Wang, Cell mechanics: mechanical response, cell adhesion and molecular deformation, *Annu. Rev. Biomed. Eng.*, 2000, **2**, 189-226.

V. Zieglschmid, C. Hollmann, and O. Bocher, "Detection of disseminated tumor cells in peripheral blood," *Crit. Rev. Clin. Lab. Sci.*, vol. 42, pp. 155-196, 2005.

Detachment of captured cancer cells under flow acceleration in a bio-functionalized microchannel

Luthur Siu Lun Cheung,[a] Xiangjun Zheng,[a] Ashley Stopa,[b] James C. Baygents,[b] Roberto Guzman,[b] Joyce A. Schroeder,[cef] Ronald L. Heimark[def] and Yitshak Zohar[aef]

Received 10th December 2008, Accepted 2nd March 2009
First published as an Advance Article on the web 18th March 2009
DOI: 10.1039/b822172c

Attachment, deformation and detachment of N-cadherin expressing prostate and breast cancer cell lines in a functionalized microchannel under hydrodynamic loading have been studied. N-cadherin antibodies are immobilized on the microchannel surface to capture the target cancer cells, PC3N and MDA-MB-231-N, from a homogeneous cell suspension. Although difficult, a significant fraction of moving cells can be captured under a low flow rate. More than 90% of the target cells are captured after a certain incubation time under no flow condition. The mechanical response of a captured cancer cell to hydrodynamic flow field is investigated and, in particular, the effect of flow acceleration is examined. The observed cell deformation is dramatic under low acceleration, but is negligible under high acceleration. Consequently, the detachment of captured cells depends on both flow rate and flow acceleration. The flow rate required for cell detachment is a random variable that can be described by a log-normal distribution. Two flow acceleration limits have been identified for proper scaling of the flow rate required to detach captured cells. A time constant for the mechanical response of a captured cell, on the order of 1 min, has been identified for scaling the flow acceleration. Based on these acceleration limits and time constant, an exponential-like empirical model is proposed to predict the flow rate required for cell detachment as a function of flow acceleration.

1. Introduction

Prostate and breast cancer are common malignancies in men and women respectively.[1] Prostate and breast cancer progression is characterized by cells that invade locally and metastasize to nearby tissues or spread throughout the body.[2] Cancer cells metastasize to other parts of the body through the blood stream or the lymphatic system and may remain latent or undetected for years.[3] Currently, there are standardized tests or examinations for the clinical diagnosis of primary prostate and breast cancer, *e.g.*, serum prostate specific antigen (PSA), digital rectal examination, mammography, ultrasonography and needle biopsy.[4–6] Since therapeutic treatment options for metastatic prostate and breast tumors are limited, early diagnosis is a critical factor in determining effective cancer treatments and survivorship. In addition, the availability of a sensitive and quantitative method for micrometastases detection, or detecting cancer cells circulating in the blood stream or body fluids, can significantly aid clinicians in designing cancer treatment plans that will improve patient prognosis, chance of survival and quality of life.

[a]*Dept. of Aerospace and Mechanical Engineering, The University of Arizona, Tucson, USA*
[b]*Dept. of Chemical and Environmental Engineering, The University of Arizona, Tucson, USA*
[c]*Dept. of Molecular and Cellular Biology, The University of Arizona, Tucson, USA*
[d]*Dept. of Surgery, The University of Arizona, Tucson, USA*
[e]*Arizona Cancer Center, The University of Arizona, Tucson, USA*
[f]*BIO5 Institute, The University of Arizona, Tucson, USA*

Circulating tumor cells (CTCs) have been identified in peripheral blood from cancer patients, and are probably the origin of intractable metastatic disease.[7,8] These CTCs are very rare in blood and, thus, their isolation presents a formidable technical challenge.[9] Nonetheless, CTCs represent a potential alternative to invasive biopsies for monitoring of non-haematologic cancers;[10] hence, the ability to characterize circulating tumor cells could assist the discovery of cancer bio-markers and enhance the understanding of metastasis. This will require not only the separation of target cells from a complex cell mixture, but also the subsequent transport and manipulation of the isolated cells for further analysis.

Microfluidic systems provide unique opportunities for cell sorting and rare-cell detection; they have been applied for flow cytometry, continuous size-based separation, and adhesion-based separation.[11] Requiring less expensive equipment and providing superior observation capabilities, microfluidic devices have been extensively used to study cell capture under different flow conditions.[12–14] Several groups have utilized antibody-based microfluidic devices for cancer cell detection in suspensions.[10–15] The methodology, in general, involves derivatization of surfaces with antibodies that are specific to the target cancer cells. This is accomplished by covalently attaching the Fc region of the antibodies onto a microchannel surface; by binding to certain proteins, the Fc region ensures proper orientation such that each antibody binding site is directed away from the channel surface. Small sample volumes are then driven through the functionalized microchannels to capture target cells from the flowing suspensions by the immobilized antibodies. In a landmark study, using anti-epithelial-cell-adhesion-molecule (EpCAM) antibody

coating, a microchannel with microposts has been developed for selective separation of viable circulating tumor cells from peripheral whole blood samples.[15] Anti-EpCAM provides the specificity for CTCs captured from unfractionated blood because EpCAM is frequently overexposed in various carcinomas such as prostate and breast, but is absent from haematologic (blood) cells.[16,17] In a similar approach, we utilized cadherin antibodies to capture specific target cancer cells. Cadherins make up a family of trans-membrane cell–cell adhesion molecules; and, one cadherin subtype interacts only with its counter receptor.[18] Many cancer cells typically down-regulate E-cadherin and up-regulate N-cadherin.[20,21] Therefore, the microchannels have been functionalized with N-cadherin antibodies to specifically capture prostate and breast cancer cells.

Two essential parameters determine the efficiency of cell capture in a functionalized microchannel surface: (i) suspension flow rate that affects the duration of cell–surface contact, and (ii) hydrodynamic loads that push cells against binding forces. These parameters must therefore be optimized to ensure maximum cell attachment. Moreover, capture of target cells in a microchannel includes cell detachment, most likely under hydrodynamic loading, enabling its transport to a certain location for further analysis. Attachment and detachment of cells on modified microchannel surfaces has been reported, including a theoretical model for fitting the experimental detachment data. The model predicts that the number of attached cells decreases exponentially with increasing wall shear stress.[22]

A common technique to measure cadherin–cadherin binding forces involves immobilizing a single cell on a micro cantilever beam and mechanically pulling it away by contact to another cell.[23] While the bond dissociation rate is reported to depend on the hydrodynamic loading level,[24,25] the rupture force of cadherin mediated binding depends on the loading rate.[26] The cell mechanical response to an external force is loading-rate dependent as well,[27–29] and a homogeneous standard linear viscoelastic solid model is popularly used to describe cell deformation due to mechanical loading.[28–34] Since cellular adhesions are often mediated *via* a small number of receptor–ligand bonds, the adhesion as well as detachment force is a random variable. The distribution function of cell detachment force depends on the number of participated binding sites,[35] and a probabilistic kinetic theory suggests a broaden distribution especially at a slow loading rate.[27] We previously suggested that cell detachment depends on both flow rate and acceleration.[36,37] Here, we explore cadherin–antibody interaction including attachment, deformation and particularly the detachment of target cancer cells, prostate and breast, under hydrodynamic loading in an antibody-functionalized microchannel.

2. Methodology

2.1 Microfluidic device fabrication

Schematic cross-sections of the major device fabrication steps are shown in Fig. 1. The fabrication process starts with the construction of a microchannel mold.[37] A 0.3 μm thick oxide layer is thermally grown on a 4″ <100> P-type silicon wafer about 500 μm in thickness, Fig. 1(a). The microchannel pattern is transferred to the oxide etch mask utilizing standard photolithography and etching techniques; the microchannel is about $L = 32$ mm long and $W = 1$ mm wide. The silicon substrate is etched in 25% tetramethylammonium hydroxide (TMAH) solution to form the microchannel mold. By using a high precision profilometer, the average height of microchannel is measured as $H = 100\ \mu m \pm 0.5\ \mu m$. After stripping the oxide etch mask, Fig. 1(b), de-molding agent (OmniCoat from MicroChem Corp.) is spin-coated to suppress adhesion forces. Polydimethylsiloxane (PDMS) solution with a mixture of 10 : 1 base to curing agent is next poured on the fabricated mold and cured at 100 °C for 1 hr, Fig. 1(c). After peeling it off the mold, holes are drilled through the cured PDMS substrate for channel inlet/outlet followed by adaptors attachment, Fig. 1(d). Then, the PDMS substrate is treated in air plasma to render its bonding surface hydrophilic. Finally, the treated PDMS substrate is bonded to a flat silicon wafer with a 0.3 μm thick thermal oxide layer to complete the process, Fig. 1(e).

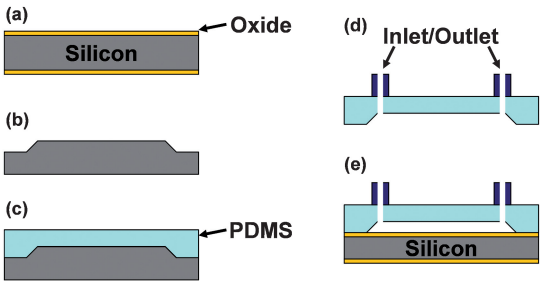

Fig. 1 Cross-sectional schematics illustrating the major steps in the fabrication of the microfluidic device.

2.2 Microchannel surface coating with antibodies

The immunoassay used to functionalize the channel surface with antibodies, previously described,[38,39] is illustrated in Fig. 2. Briefly, the microchannel is filled with 1% (vol/vol) 3-aminopropyltriethoxysilane (APTES from Sigma)–acetone solution for 15 min at room temperature. The APTES-coated surface is activated with 2% (vol/vol) glutaraldehyde in water (Fluka) for 2 hr at room temperature to promote a Schiff-base reaction. After flushing the microchannel with excess of distilled water and 1× phosphate buffered saline (PBS) solution, recombinant protein G from *E. coli* (Zymed Lab Inc.), at a concentration of 50 μg ml^{-1} in 1× PBS, is incubated on the activated surface overnight at 4 °C. In order to block excess of silanol sites, the channel is filled with bovine serum albumin (BSA from Sigma) solution (2 mg ml^{-1} in 1× PBS) for 1 hr at room temperature. N-cadherin (Clone GC-4 from Sigma) antibodies from mouse, 100 μg ml^{-1} in 1× PBS, are then incubated on the protein G layer

Fig. 2 A schematic illustration of the immunoassay used for immobilizing antibodies on a microchannel surface.

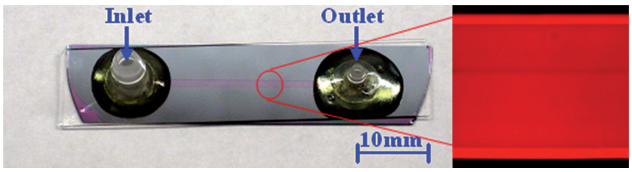

Fig. 3 A photograph of a packaged microdevice with a fluorescent microscope image indicating the uniform bio-activity of the immobilized antibodies.

at room temperature for 1 hr. The immunoassay is finally completed by washing the microchannel with PBS solution. Since the antibody surface concentration could be an important factor, the surface has been saturated by incubation in a solution with high antibody concentration. In an earlier work, using trypsin to replace the protein G and N-cadherin antibody pair, the surface density was estimated to be 10^{12} molecules cm^{-2}.[39] This seems to be an upper limit for the antibody surface density which, based on initial results, is on the order of 10^{11} molecules cm^{-2}.

The bio-activity of the antibody layer inside the microchannel, after device packaging, is tested using antibody–antigen interaction. Anti-mouse IgG whole molecules (Jackson ImmunoResearch), at a concentration of 15 μg ml^{-1} in 1× PBS and tagged with Cy3 fluorescent dyes, are incubated in the microchannel for 1 hr at room temperature in the dark to prevent photo bleaching of the Cy3 molecules. After incubation, the microchannel is washed thoroughly and filled with 1× PBS. The device is then placed under a fluorescent microscope (Nikon eclipse 80*i*) equipped with Cy3 filter; the excitation and emission wavelength is 550 and 570 nm, respectively. A photograph of a fabricated microfluidic device is shown in Fig. 3; the image next to it, showing uniform intensity of the emitted red light, indicates uniform antibody activity on the microchannel surface.

2.3 Cell culture

Two types of cancer cells, prostate and breast, are utilized in this work. PC3N prostate cancer cell line, expressing N-cadherin and lack of E-cadherin, is maintained and grown in 1× DMEM/F12 (Dulbecco's modified Eagle's medium with 1 : 1 Ham's F12 medium, Invitrogen) with 10% fetal bovine serum (Cellgro) and 1% penicillin–streptomycin (Invitrogen) in humid environment at 37 °C and 5% CO_2.[19] Prior to experiments, the growth medium is aspirated and the cells are incubated with 4 mM ethylenediaminetetraacetic acid (EDTA) in calcium and magnesium free PBS (CMF-PBS) for 20 min for detachment. After centrifugation and solution removal, the cells are re-suspended in 1× CMF-PBS, while the concentration is determined by cell counting with a haemocytometer; the suspended cell diameter is about $D = 20$ μm. The PC3N cell suspension is immediately loaded into a functionalized microchannel for experimentation.

In order to study the cell type effect on cell capture and detachment, breast cancer cell line MDA-MB-231 is selected for the present experiments as it is widely used as a model of metastatic disease;[40,41] however, these cells endogenously express cadherin-11. It is important to keep all parameters constant, including the particular cadherin–antibody combination, to allow a proper comparison between different cell types. Hence, the original cells are transfected with a N-cadherin expression vector to enable capture of breast cancer cells in microchannels functionalized with the same N-cadherin antibodies. The complete coding sequence (906 amino acids) of human N-cadherin (NM001792) was amplified by PCR (polymerase chain reaction) using a full length N-cadherin cDNA as a template,[42] and cloned in frame with EGFP (enhanced green fluorescent protein) in the vector pEGFPN1 (Clonetech). The N-cadherin EGFP fusion was verified by sequencing. The resulting plasmid pN-cadherinEGFP was linearized and transfected into MDA-MB-231 cells (ATCC) using Fugene6 (Roche). Following selection with Neomycin (Invitrogen) at 800 μg ml^{-1}, the pools of stable clones of MDA-MB-231-N cells were utilized for the studies. More than 95% of the MDA-MB-231-N cells expressed N-cadherinEGFP. The transfected MDA-MB-231-N breast cancer cells, about 15 μm in diameter, are maintained and grown under the same conditions as the PC3N cells with the addition of antibiotic G418 sulfate (Invitrogen) at concentration of 800 μg ml^{-1}.

2.4 Experimental set-up

All experiments are conducted and monitored using a probe station (Signatone S-1160) equipped with a microscope (Motic microscope PSM-1000), a CCD camera and a DVD recorder (Panasonic DMR-E85H) for further data processing. The prepared cancer cell suspension is loaded through an antibody-functionalized microchannel using a syringe pump (WPI Inc. SP100i). Once the proper number of cells is loaded, about 1500, the syringe is effectively separated from the channel. The number of cells present in the microchannel is then counted as the initial condition. Dilute cell suspensions have been used in all experiments, at a concentration below 5×10^5 cells ml^{-1}, ensuring that all cells present in the microchannel contact the channel surface with minimum cell–cell interaction.

A high performance liquid chromatography (HPLC) pump (Shimadzu LC-20AD), featuring programmable flow acceleration, is used to remove un-bounded cells and conduct cell detachment experiments under a finely controlled flow rate. All data in this report are given in terms of volume flow rate, Q; and dividing it by the channel cross-sectional area yields the average flow velocity, $U = Q/(W \cdot H)$. The wall shear stress, τ_w, is often utilized to represent the hydrodynamic loading. Assuming 2-D flow, since $W \gg H$, the wall shear stress is also directly proportional to the flow rate given by:

$$\tau_w = \frac{6Q\mu}{WH^2} \quad (1)$$

where $\mu = 1 \times 10^{-3}$ kg m^{-1} s^{-1} is the viscosity of the PBS working fluid.[43]

3. Target cell capture in an antibody-functionalized microchannel

Surfaces immobilized with antibodies are used to capture target cells from a suspension similar to other studies.[13,15] Cadherins make up a family of cell–cell adhesion molecules (receptors) and, in contrast with other trans-membrane receptors, adhesion of cadherins is homotypic; one cadherin subtype interacts only with

an identical counter receptor. Therefore, since both PC3N and MDA-MB-231-N lines consist of cells with N-cadherin molecules, the microdevices are functionalized with N-cadherin antibodies for specific binding.

To demonstrate the binding specificity of an anti-N-cadherin coated surface, four different cell lines, PC3N (N-cadherin), BT20 (E-cadherin), MDA-MB-231 (cadherin-11) and transfected MDA-MB-231-N (N-cadherin) suspended in CMF-PBS, have been incubated on an anti-N-cadherin coated surface for 15 min. More than 90 ± 3% of N-cadherin expressing cells (PC3N and MDA-MB-231-N) were captured, while less than 10 ± 3% of the other cell types (BT20 and MDA-MB-231) were captured. Furthermore, less than 10 ± 1% of N-cadherin expressing cells (PC3N) were captured on a surface coated with different antibodies (mouse IgG). This clearly demonstrates that the current cadherin–antibody system results in specific binding, and changing either the cell or the coating type will result in poor capture ratio. A separate experiment, in which the buffer was changed from CMF-PBS to Dulbecco's phosphate buffered saline (D-PBS contains calcium), showed no difference in the capture efficiency as a function of the two buffer constituents. The only reason for using calcium-free buffer in these experiments was to minimize cell cluster formation by suppressing cell–cell adhesion.

3.1 Incubation time effect on cell capture rate

Cell–surface interaction requires a certain time to attain a strong bond. To test the effect of incubation time, PC3N cells have been incubated in anti-N-cadherin functionalized microchannels at room temperature, under no flow condition, for various time periods. The cell suspension is loaded using the syringe pump and, once the microchannel is full, the pump is turned off. All PC3N cells sink to the channel bottom surface within a few seconds, due to their higher density relative to the solution; this ensures a direct contact between each cell and the functionalized surface. The number of PC3N cells present in the microchannel is then counted (N_i), while allowing cell incubation for a certain time period. Then, the HPLC pump is used to flush the microchannel with 1× CMF-PBS, for 3 min under a flow rate of 0.0083 ml min^{-1}, to remove un-bounded cells. The number of the remaining PC3N cells, firmly attached to the functionalized surface, is counted (N_0) after channel washing for each incubation-time period. The fraction of captured cells, with respect to the initial number of cells loaded into each channel, is plotted in Fig. 4. The fraction of captured PC3N cells, firmly bound to the N-cadherin antibodies immobilized on the channel surface, increases rapidly with increasing incubation time. Incubation for at least 5 min is needed to secure firm attachment of practically all PC3N cells initially loaded into the microchannel. The effect of incubation time on the capture rate of MDA-MB-231-N has also been tested as shown in Fig. 4; similar to the PC3N cells, almost all the cells are captured within 5 min incubation time.

The initially suspended cancer cells are uniformly distributed in the microchannel; hence, the measured incubation time necessarily includes the time it takes the suspended cells to settle on the functionalized bottom surface. To estimate this settling time, the cell settling velocity has been measured and found to be about 10 μm s^{-1}; thus, within a 100 μm high microchannel, each cell should come into full contact with the antibody-functionalized bottom surface in less than 10 s. Therefore, the much longer incubation time scale of about 5 min is required for establishing a strong bond between the settled cells and the immobilized antibodies.

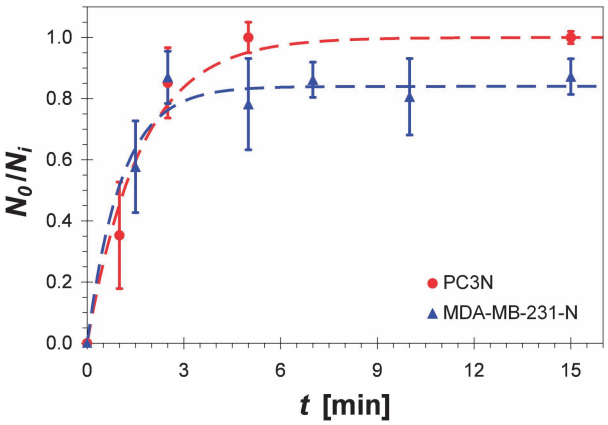

Fig. 4 The effect of incubation time on the percentage of cancer cells captured on an anti-N-cadherin coated microchannel surface.

3.2 Target cell capture from a flowing homogenous cell suspension

Experiments have been conducted to capture target cells from a suspension flow with the aim of isolating CTCs from the blood stream. Prepared PC3N cell suspensions are driven through anti-N-cadherin functionalized microchannels at constant flow rates adjusted by the HPLC pump. Although attempts to capture moving cancer cells under a high flow rate have not been successful, capture of cells at a relatively low flow rate of 0.001 ml min^{-1} has been demonstrated; this is the lowest stable flow rate that can be obtained by the available pump. The time-dependent displacement of the cell Δx is directly measured from the recorded images, while the cell velocity V is calculated as the time derivative of its displacement. Both the location and velocity of the PC3N cell are plotted in Fig. 5. The cell velocity drops from about 75 μm s^{-1} to zero, over a distance of about 75 μm in less

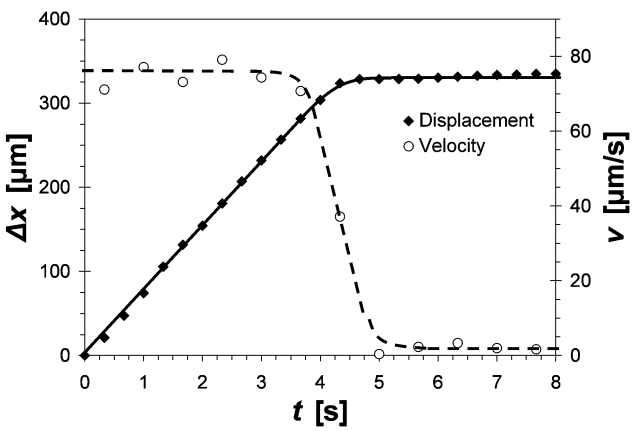

Fig. 5 Displacement and velocity of a particular PC3N cancer cell exhibiting complete stop that indicates capture.

than 2 s, as it comes to a halt allowing local interaction with the antibodies immobilized on the channel surface. It is important to note that even at this low flow rate, only about half of the loaded PC3N cells are captured while the rest keep rolling on the bottom surface toward the channel exit.

4. Captured cell response to hydrodynamic loading

The cell-attachment results indicate that a minimum of 5 min incubation time is required to bind almost all PC3N or MDA-MB-231-N cells onto the antibody-functionalized channel surface. Since both the cell suspensions and the functionalized microchannels contain random experimental uncertainties, a conservative 15 min incubation time has been selected for studying the response of captured cells subject to an applied shear flow.

4.1 Experimental conditions

Once the binding between the cells and the functionalized surface is established, a certain level of fluid energy/flow rate is required to detach cells. However, the same flow rate Q can be obtained within different time intervals depending on the flow acceleration dQ/dt imposed by the pump setting. Here, flow acceleration is strictly defined as the flow rate increase with time, $dQ/dt > 0$, different from convective acceleration that accounts for spatial gradients of the velocity field. Several flow acceleration levels have been tested and, for demonstration, only two cases corresponding to $dQ/dt = 0.33$ ml min^{-2} (denoted as A) and 0.033 ml min^{-2} (denoted as B) are sketched in Fig. 6. The tested flow conditions are represented by A_{jk} and B_{jk}; where the subscript $j = 1,2, \ldots, n$ denotes the flow rate level, and $k = 1,2$ denotes the start and finish of the following constant flow rate interval respectively. The HPLC pump is programmed to linearly increase the flow rate with time from zero to a desired level (solid lines connecting the origin with points A_{j1} & B_{j1}). Once the design flow rate is achieved, the pump maintains the flow rate constant for additional 5 min to obtain a steady state (dash lines connecting points A_{j1} & B_{j1} with A_{j2} & B_{j2}). At the end of the constant flow rate interval, the pump is shut down bringing the flow back to rest.

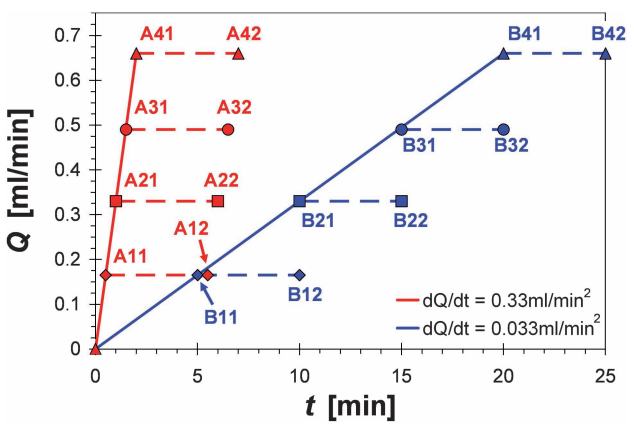

Fig. 6 A summary of two example experimental conditions, high (red) and low (blue) flow acceleration, under which cell detachment has been examined; symbols represent instances at which either the flow acceleration (A_{j1} & B_{j1}) or the flow rate is switched off (A_{j2} & B_{j2}).

4.2 Captured-cell deformation

As the flow accelerates, an attached cell experiences hydrodynamic loads (force and moment) increasing with time and, in response, the cell is deformed. To demonstrate the effect of flow acceleration on cell deformation, video clips of captured PC3N cells under accelerating flow rates have been recorded. Extracted images of the deformed cells for high, 0.33 ml min^{-2}, and low acceleration, 0.033 ml min^{-2}, are shown in Fig. 7(a) and (b) respectively. As expected, since a captured cell having a flexible membrane is anchored, it deforms under the applied hydrodynamic load. Interestingly, though, the deformed cell shape depends not only on the actual flow rate Q but also on the preceding flow evolution, *i.e.* flow acceleration dQ/dt. Under high flow acceleration (from origin to points A_{j1}), the spherical shape of the captured cell remains practically the same regardless

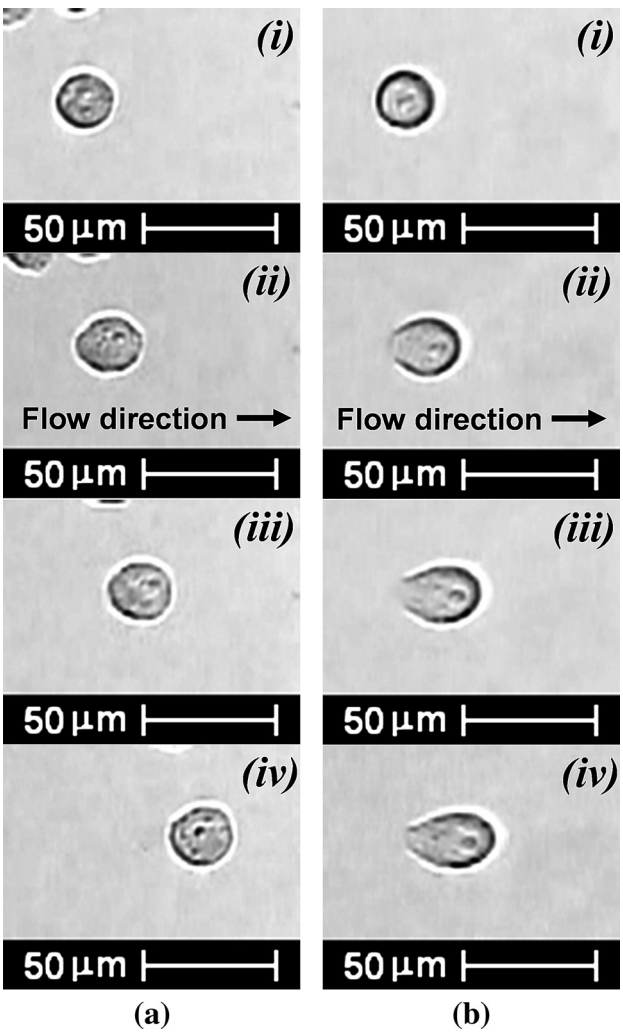

Fig. 7 Image sequences of PC3N cell deformation under the flow acceleration conditions illustrated in Fig. 6: (a) 0.33 ml min^{-2} and (b) 0.033 ml min^{-2}. The instantaneous flow rates are: (i) no flow, (ii) 0.175 ml min^{-1}, (iii) 0.33 ml min^{-1} and (iv) 0.45 ml min^{-1}.

of the instantaneous flow rate as shown in Fig. 7(a); a slight increase in the cell projected area, as the flow rate increases, is accompanied by a finite rolling motion of the captured cell in the streamwise direction. In contrast, under low flow acceleration (from origin to points B_{fl}), the captured cell is deformed and elongated by the shear flow resulting in a tear-drop shape as shown in Fig. 7(b). The cell is stretched downstream from its initial length of about 20 μm at $Q = 0$ ml min^{-1} to about 35 μm at $Q = 0.45$ ml min^{-1}, with very little change in its width of about 20 μm in the spanwise direction.

Using a Matlab image processing program, the cell projected area A is measured from images similar to those shown in Fig. 7. The cell area, normalized by its initial area under zero flow rate A_0, is plotted in Fig. 8 as a function of the instantaneous flow rate for both flow accelerations. Under low acceleration, the cell projected area initially increases almost linearly with flow rate, up by about 30% at $Q = 0.25$ ml min^{-1}. Then, the deformation rate is slowly leveled off approaching a larger projected area by about 40% at $Q = 0.4$ ml min^{-1}. In comparison, under high acceleration, the cell retains its projected circular area increasing slightly in size by about 15% at $Q = 0.5$ ml min^{-1}. Increasing the flow rate further, $Q > 0.5$ ml min^{-1}, results in detachment of almost all the captured cells.

The dramatic difference in cell deformation under the same flow rate due to varying flow acceleration is consistent with the well-documented viscoelastic behavior of biological cells. A homogeneous standard linear solid (SLS) model has been proposed to describe cell response to external mechanical loading.[28,34] The model contains a damping element controlling the deformation rate, and a damping mechanism explicitly implies that a cell requires a finite time to deform in response to mechanical loads.[29] Therefore, when a mechanical load is applied within a short period of time, as in high acceleration, the cell cannot respond simply retaining its original shape similar to a solid object. On the other hand, under low acceleration when the loading is slowly ramped up, the cell has enough time to completely deform as a compliant material in a quasi-steady manner. Although the cell viscoelastic property has previously been associated with micropipette aspiration and mechanical indentation,[31,32,34] the present results verify this behavior in cell response to hydrodynamic loading as well. Hence, flow acceleration should be a critical control parameter in determining the captured-cell response to fluid flow in a microchannel.

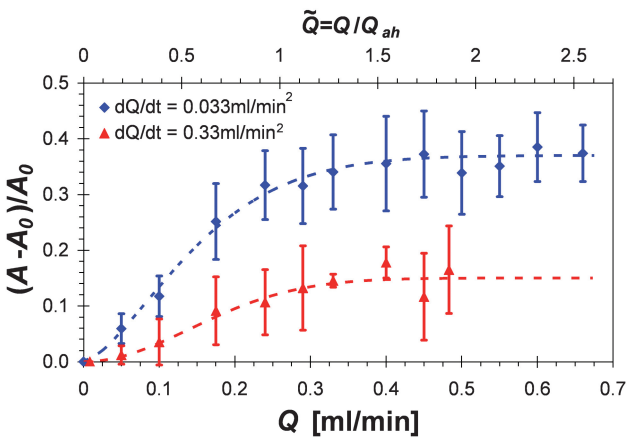

Fig. 8 The dependence of the cell projected area (top view), normalized by its initial area, on the instantaneous flow rate for both low and high acceleration.

5. Cell detachment under accelerating shear flow

Assuming the cell volume is conserved during the relatively short flow-acceleration experiments (less than 30 min); increased projection area due to hydrodynamic loading necessarily entails a decrease in the cell height. Following a proposed geometric model for a captured cell subject to shear flow,[44] the height of a tear-shaped cell is about half the height of the original hemispherical cell under no flow. The lower cell profile in turn results in reduced hydrodynamic loads. Thus, under lower flow acceleration, captured cells experience lower hydrodynamic loads when exposed to the same flow rate. Consequently, even assuming constant cell–surface binding force, higher flow rate will be required to detach such highly-deformed cells. Furthermore, the cell adhesion force to the antibody-functionalized surface may not stay constant. It is plausible to assume that the number of binding sites is approximately proportional to the cell contact area; and, since a cell projected area under lower acceleration is larger, the cell adhesion force might also be larger. Consequently, a higher flow rate would be required to detach a captured cell subject to lower flow acceleration due to both lower profile, leading to lower hydrodynamic loading, and larger contact area, resulting in higher binding force.

Detachment of PC3N cells bound to an anti-N-cadherin functionalized surface due to applied shear flow in a microchannel has been investigated focusing on the effect of flow acceleration. To this end, different flow acceleration levels have been tested including a 'step function' case, in which the flow rate is increased as fast as the mechanical pump allows ($dQ/dt = 4.5$ ml min^{-2}). In each test, the prepared PC3N cell suspension is loaded into a functionalized microchannel, followed by 15 min incubation time. After washing, the number of captured cells N_0 is counted and, usually, it is equal to the number of initially loaded cells N_i. Next, the flow rate increases linearly with time (dQ/dt = const) from zero until a prescribed flow rate Q is obtained; several flow rates have been selected for each of the tested flow acceleration. This is followed by a 5 min interval of constant flow rate, *i.e.* $dQ/dt = 0$, to establish steady-state conditions. The pump is then turned off, at the end of the constant flow rate stage, and the number of the remaining captured cells N_a is counted. The number of detached cells, $N = N_0 - N_a$, normalized by the initial number of captured cells, N_0, is plotted in Fig. 9(a) as a function of the normalized prescribed flow rate for all tested flow accelerations; the flow rate required for removing half of the captured cells under 'step function' flow acceleration, $Q_{ah} = 0.26$ ml min^{-1}, is chosen for flow rate scaling.

All curves start at the origin as no cell can be detached under no flow condition ($Q = 0$). With increasing flow rate, the fraction of detached cells increases gradually towards unity indicating complete removal of all initially captured cells. If all captured cells are identical, *i.e.* having the same number of binding sites with the same bond strength, then all cells should be detached at the lowest flow rate above which the hydrodynamic loads overcome the adhesion forces. However, the cells vary among themselves in size and membrane properties, while the

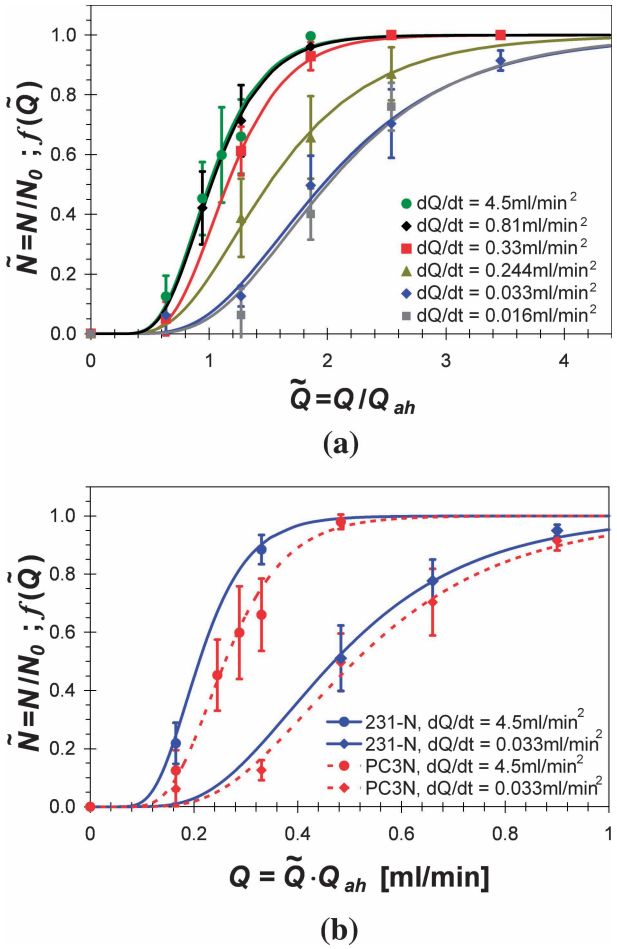

Fig. 9 (a) A comparison between the measured fraction of detached PC3N cells as a function of the applied flow rate (symbols) and fitted log-normal probability distribution functions calculated based on eqn 2 (curves) for various flow accelerations; and (b) a comparison between the limiting flow accelerations, 'step function' and 'quasi-steady', for the PC3N and the MDA-MB-231-N cells.

antibody-coated surfaces and the applied shear flows are not perfectly uniform as well. Consequently, the cell–surface binding force is randomly distributed within a certain range, requiring different flow rates to detach various captured cells as has been observed. However, if only the flow rate level is relevant in determining the hydrodynamic loads on a captured cell, all the results in Fig. 9(a) should collapse into a single curve regardless of flow acceleration. It is clearly not the case as the fraction of detached cells monotonically increases with increasing flow acceleration under the same flow rate; *e.g.*, at $Q = 2Q_{ah}$, the fraction of detached cells increases from about 0.4 under 0.016 ml min^{-2} to about 0.95 under 0.81 ml min^{-2} acceleration. This indicates that flow acceleration affects both the hydrodynamic loads and the adhesion forces experienced by a captured cell under a certain flow rate consistent with the cell deformation results.

An interesting feature of the data shown in Fig. 9(a) is the apparent lower bound on the flow acceleration, below which the effect of flow acceleration vanishes; the curves corresponding to $dQ/dt = 0.033$ ml min^{-2} and 0.016 ml min^{-2} are the same within experimental error. This lower bound limit represents a 'quasi-steady' cell behavior, in which the cell has sufficient time to fully respond to the instantaneous flow field as in a steady-state flow. Lowering further the flow acceleration rate, $dQ/dt < 0.016$ ml min^{-2}, will result in a similar response depending only on the flow rate. On the other hand, the 'step function' acceleration represents an upper bound limit. Since the cell has no time to respond, its detachment must depend only on the instantaneous flow rate. Indeed, increasing the flow acceleration level from $dQ/dt = 0.81$ ml min^{-2} to 4.5 ml min^{-2} results in the same cell detachment rate.

The effect of flow acceleration on detachment of MDA-MB-231-N cells, bound to an anti-N-cadherin functionalized surface, has also been investigated. Similar behavior has been observed and, for clarity, only the fraction of detached cells under the upper and lower flow acceleration bounds are compared in Fig. 9(b) with the corresponding PC3N results. The only difference between the two sets of data is the slight shift of the MDA-MB-231-N results to the left; namely, to detach the same fraction of captured cells, MDA-MB-231-N cells require lower flow rate than PC3N cells. This may indicate that the binding of the smaller MDA-MB-231-N cells ($D \sim 15$ μm) is weaker than the binding of the larger PC3N cells ($D \sim 20$ μm). If so, the apparent weaker binding of MDA-MB-231-N cells could perhaps be due to a smaller cell–surface contact area.

5.1 Statistical modeling of cell-detachment kinetics

Each curve in Fig. 9(a,b) in fact represents a cumulative distribution function bound between 0 and 1. The varying flow rate required for cell detachment can be thought of as a product of several independent and random factors, *e.g.* binding forces and hydrodynamic loads. Hence, the cell-detachment flow rate can statistically be modeled as log-normal, and the following probability distribution function f is fitted to each flow acceleration data set:

$$f(\tilde{Q};\mu,\sigma) = \frac{1}{2} + \frac{1}{2}\mathrm{erf}\left[\frac{\ln\tilde{Q} - \mu}{\sigma\sqrt{2}}\right] \quad (2)$$

with μ and σ, the mean and standard deviation of the flow rate natural logarithm, being the fitting parameters. The normalized variables and the mean distribution are defined as:

$$\tilde{N} = \frac{N}{N_0};\ \tilde{Q} = \frac{Q}{Q_{ah}};\ \mu = \ln\left(\frac{Q_a}{Q_{ah}}\right) \quad (3)$$

For convenience, Q_a is selected as the flow rate required for detachment of half of the captured cells; thus, the standard deviation is the only free parameter adjusted to obtain the best fit of eqn 2 depending on the flow acceleration. The pairs of fitting parameters, Q_a/Q_{ah} and σ, determined for PC3N cells under all tested flow accelerations are listed in Table 1.

The agreement between the fitted probability distribution functions and the measured experimental results in Fig. 9(a,b) indicates both: the suitability of the log-normal statistical model to analyze the cell detachment results, and the proper selection of the scaling parameters. Therefore, though difficult to confirm experimentally, it should be interesting to examine the complimentary probability density function g for a log-normal distribution; it is readily available by differentiating the probability density function in eqn 2, with respect to the normalized flow rate, as follows:

Table 1 The parameters used to fit the log-normal cumulative distribution functions to the measured fraction of detached PC3N cells for various flow accelerations

	Flow acceleration, dQ/dt					
	0.016 ml min^{-2}	0.033 ml min^{-2}	0.244 ml min^{-2}	0.33 ml min^{-2}	0.81 ml min^{-2}	4.5 ml min^{-2}
Q_a [ml min^{-1}]	0.52 (Q_{as})	0.51	0.39	0.30	0.265	0.26 (Q_{ah})
Q_a/Q_{ah}	2.00	1.96	1.50	1.15	1.02	1.00
σ	0.43	0.45	0.46	0.34	0.35	0.35
θ [min]	16.25	7.879	1.066	0.788	0.321	0.058

$$g(\tilde{Q};\mu,\sigma)=\frac{df}{d\tilde{Q}}=\frac{1}{\tilde{Q}\sigma\sqrt{2\pi}}\exp\left[-\frac{(\ln\tilde{Q}-\mu)^2}{2\sigma^2}\right] \quad (4)$$

The resulting curves, based on eqn 4, are plotted in Fig. 10(a,b) for each acceleration flow depicted in Fig. 9(a,b). As the flow acceleration decreases, for the two cell types PC3N and MDA-MB-231-N, the peak shifts to a higher flow rate with a wider distribution; *i.e.* both μ and σ decrease with increasing dQ/dt. Log-normal distributions have also been observed in measurements of strength of bonds between biological receptor molecules and their ligands,[24] as well as in measurements of forces required for rapid detachment of agglutinin-bonded red blood cells.[35] These results led to the notion that the number of binding sites of a captured cell is a discrete, time-dependent, random variable with significant fluctuations; thus, a probabilistic theory has been applied to describe the state of such systems.[27] Consistent with the distributions depicted in Fig. 10(a,b), both the rupture force (equivalent to flow rate) and its standard deviation are reported to increase with either increasing number of bonds (equivalent to contact area) or decreasing force loading rate (equivalent to flow acceleration).

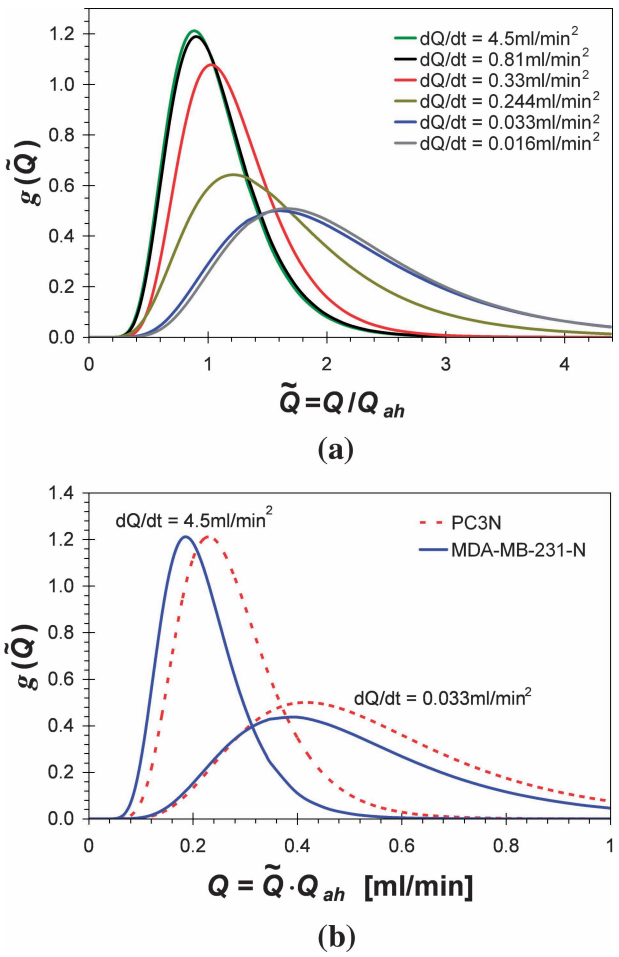

Fig. 10 (a) The log-normal probability density functions of PC3N cells detached from an anti-N-cadherin functionalized microchannel calculated based on eqn 4 for the probability distribution functions plotted in Fig. 9(a); and (b) the probability density functions for captured PC3N and MDA-MB-231-N cell subject to the 'step function' and 'quasi-steady' accelerations corresponding to Fig. 9(b).

5.2 Acceleration effect on the flow rate required for cell detachment

The cell detachment results indicate that, under the same flow rate, the fraction of detached cells strongly depends on the loading rate (flow acceleration). This can be viewed as a balance between two competing time scales; a detachment-force time scale determined by the externally-applied flow acceleration and a cell-deformation time scale depending on the inherent cell physiology. The characteristic time scale for the hydrodynamic loading depends on the applied accelerating flow, dQ/dt, and it is normalized by the characteristic flow rate Q_{ah} to obtain the correct dimensions of time as follows:

$$\theta=\left(\frac{1}{Q_{ah}}\frac{dQ}{dt}\right)^{-1} \quad (5)$$

This scaling represents the ramping-up time needed for the flow rate to reach the required level of $Q = Q_{ah}$ under various flow accelerations as listed in Table 1; these data can now be used to estimate the time scale for the cell mechanical response. The fitted standard deviation for PC3N is plotted in Fig. 11 as a function of the normalized flow acceleration. The results are grouped around two levels, 0.35 for relatively high and 0.45 for low flow acceleration, with a sharp jump between them. The lower standard deviation at high acceleration is mainly due to the initial randomness of the cell–surface binding force after incubation. However, due to the cell deformation under low flow acceleration, the randomness in the cell–surface binding forces increases with increasing cell projected area. Similarly, in a molecular study of a receptor–ligand binding force, both the rupture force and its standard deviation are found to increase with increasing number of binding sites.[27,35] Recalling the images shown in Fig. 7, a deformed cell under low acceleration has a larger projected area and potentially larger number of binding sites in comparison to a cell under high flow acceleration. Therefore, the time corresponding to the jump in the standard

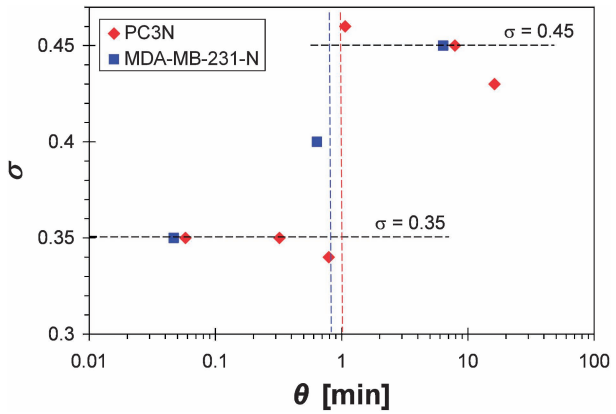

Fig. 11 The dependence of the distribution standard deviation (σ) on the flow acceleration (dQ/dt) normalized by the characteristic flow rate (Q_{ah}) showing a jump around a characteristic time scale of $\tau = 1.15$ and 0.85 min for the PC3N and MDA-MB-231-N cells, respectively.

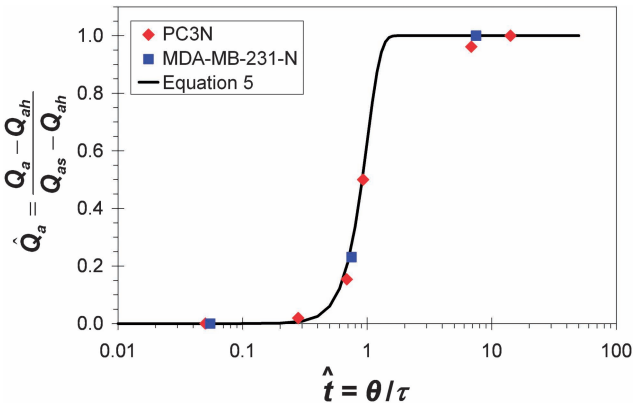

Fig. 12 A comparison between the normalized flow rate required for detachment of half of the captured cells Q_a measured as a function of the normalized flow acceleration θ (symbols), for both PC3N and MDA-MB-231-N cells, and the empirical exponential formula in eqn 6 fitted with $b = 4$ (solid line).

deviation level, $\tau = 1.15$ min, can be considered as the proper time scale characterizing the PC3N cell mechanical response to hydrodynamic loading. The characteristic time scale for MDA-MB-231-N cells is lower, $\tau = 0.85$ min, suggesting that these cells respond faster to mechanical loading.

The flow rate required for cell detachment has been analyzed in previous studies as a function of the specific cell–surface system only; however, the present results suggest that it also depends on flow acceleration. The explicit dependence of the flow rate required for detaching half of the captured cells, Q_a, on the flow acceleration, dQ/dt, should therefore be explored to quantify this effect. Two limits have been discovered in the cell detachment experiments: 'step function' acceleration, providing a lower limit $Q_a = Q_{ah}$, and 'quasi-steady' acceleration, providing an upper limit $Q_a = Q_{as}$; hence, proper scaling of Q_a should involve both limiting parameters Q_{ah} and Q_{as}. Furthermore, the cell mechanical time scale τ is utilized to render the flow acceleration dimensionless. Using these scaling arguments, the normalized flow rate required for detachment of the two cell types, PC3N and MDA-MB-231-N, is plotted in Fig. 12 as a function of the normalized flow acceleration. A simple mathematical model describing a sharp transition between two asymptotic levels is the following exponential function:[22]

$$\hat{Q}_a = \frac{Q_a - Q_{ah}}{Q_{as} - Q_{ah}} = 1 - \exp\left(-\hat{t}^b\right); \quad \hat{t} = \theta/\tau \qquad (6)$$

In this scaling, the normalized required flow rate is conveniently bound between 0 and 1 with the normalized time for the sharp transition around 1, and the only fitting parameter is the exponent b. The results for both cell types not only collapse onto a single curve but also, with $b = 4$, the agreement between the calculations and measurements is remarkable. Therefore, the reported cell detachments behavior is not limited to a particular cell type but can be extended to other cell–surface combinations. Furthermore, the empirical formula describes properly the transition from high to low flow acceleration regime characterizing the mechanical detachment of captured cells due to hydrodynamic loading.

The SLS model has originally been proposed to study small-strain deformation of living cells undergoing micropipette aspiration. The whole cell is modeled as a homogeneous linear viscoelastic solid with two elastic, k_1 and k_2, and one viscous element, η, represented by two springs and a dashpot; the characteristic time response of such a system is given by $\eta(k_1 + k_2)/(k_1k_2)$. Spring and damping constants have been measured for a variety of cells under different conditions, yielding a time constant in the range of 0.5–2 min.[28] Indeed, the estimated response time of a captured PC3N or MDA-MB-231-N cell to applied hydrodynamic loading, 1.15 and 0.85 min respectively, is well within this range. The effect of flow acceleration can now be summarized as follows: under high acceleration, $\theta < \tau$, the cell deformation is negligible resulting in high hydrodynamic loads; consequently, low flow rate is sufficient for cell detachment as $Q_a \rightarrow Q_{ah}$; under low acceleration, $\theta > \tau$, the cell deformation is significant resulting in both low hydrodynamic loads and possibly higher binding forces; thus, high flow rate is needed for cell detachment as $Q_a \rightarrow Q_{as}$.

It is important to note that Q_{ah}, Q_{as} and τ are characteristics of a particular system including cell type, surface coating, buffer solution and microchannel geometry. Varying any of these parameters will necessarily lead to a different set of values as summarized in Table 2 for PC3N and MDA-MB-231-N. Furthermore, similar to either the average velocity or the wall shear stress, the flow rate is only a representative of the hydrodynamic loading. The actual loads depend on the detailed stress distribution around the cell membrane; obtaining this stress field requires a major effort yet to be conducted. Finally, a cell viability test has been conducted using propidium iodide (PI) as

Table 2 The characteristic parameters used for the scaling of the flow rate required for cell detachment, PC3N and MDA-MB-231-N, as well as the flow acceleration

	Q_{as}/ml min^{-1}	Q_{ah}/ml min^{-1}	τ/min
PC3N	0.52	0.26	1.15
MDA-MB-231-N	0.47	0.21	0.85

a viability marker at 1 μg ml^{-1} in 1× PBS. Non-viable cells were labeled by red dye and detected under fluorescent microscope. The results show that more than 80 ± 5% of deformed cell, exposed to flow rate up to $Q = 0.5$ ml min^{-1} under flow acceleration of $dQ/dt = 0.033$ ml min^{-2}, are still viable.

6. Conclusions

A microchannel functionalized by N-cadherin antibodies has been utilized to study the behavior of a homogeneous suspension of N-cadherin expressing PC3N prostate and MDA-MB-231-N breast cancer cells subject to hydrodynamic loading. Under the minimum stable flow rate allowed by the available pump, 0.001 ml min^{-1}, about half of the flowing cells can be captured in a microchannel; however, under no flow condition, almost all suspended cells can be captured after about 5 min incubation time. Following 15 min incubation time to ensure steady-state cell–surface interaction, the effect of flow acceleration has been investigated. A captured cell maintains its spherical shape with little deformation under high flow acceleration, while it is significantly deformed attaining a tear-drop shape under low flow acceleration.

The required flow rate for cell detachment is random in nature, and is adequately described by a log-normal distribution. Two flow acceleration limits have been identified corresponding to: (i) 'step function' acceleration requiring the minimum flow rate for cell detachment with a small standard deviation, and (ii) 'quasi-steady' acceleration requiring the maximum flow rate for cell detachment with a large standard distribution. The sharp transition from the low to high standard deviation provides a time constant of about 1 min for the mechanical response of a captured cancer cell to hydrodynamic loading. Utilizing both detachment flow rate limits and the cell mechanical time constant, a unified empirical exponential function is found to adequately predict the flow rate required for cell detachment as a function of flow acceleration for both PC3N and MDA-MB-231-N cancer cells.

Acknowledgements

This work is supported by a BCRP grant, BC061859, administered by the US Army Medical Research, and by the Arizona Biomedical Research Commission grant 06-080.

References

1 A. Jemal, R. Siegel, E. Ward, Y. Hao, J. Xu, T. Murray and M. J. Thun, Cancer statistics 2008, *CA Cancer J. Clin.*, 2008, **58**, 71–96.
2 D. X. Nguyen and J. Massagué, Genetic determinants of cancer metastasis, *Nature Reviews Genetics*, 2007, **8**, 341–352.
3 M. S. Simon, D. Ibrahim, L. Newman and M. Stano, Efficacy and economics of hormonal therapies for advanced breast cancer, *Drugs Aging*, 2002, **19**(6), 453–463.
4 S. F. Sener, B. Cady and D. Merkel, Primary factor in declining breast cancer mortality rates – Early detection or adjuvant therapy?, *Cancer Pract.*, 2002, **10**(1), 45–47.
5 F. Wärnberg, H. Nordgren, L. Bergkvist and L. Holmberg, Tumour markers in breast carcinoma correlate with grade rather than with invasiveness, *Br. J. Cancer*, 2001, **85**(6), 869–874.
6 R. S. Taichman, R. D. Loberg, R. Mehra and K. J. Pienta, The evolving biology and treatment of prostate cancer, *J. Clin. Invest.*, 2007, **117**, 2351–2361.
7 M. Cristofanilli, G. T. Budd, M. J. Ellis, A. Stopeck, J. Matera, M. C. Miller, J. M. Reuben, G. V. Doyle, W. J. Allard, L. W. M. M. Terstappen and D. F. Hayes, Circulating tumor cells, disease progression, and survival in metastatic breast cancer, *N. Engl. J. Med.*, 2004, **351**, 781–791.
8 J. S. de Bono, H. I. Scher, R. B. Montgomery, C. Parker, M. C. Miller, H. Tissing, G. V. Doyle, L. W. W. M. Terstappen, K. J. Pienta and D. Raghavan, Circulating Tumor Cells Predict Survival Benefit from Treatment in Metastatic Castration-Resistant Prostate Cancer, *Clin. Cancer Res.*, 2008, **14**(19), 6302–6309.
9 H. J. Kahn, A. Presta, L.-Y. Yang, J. Blondal, M. Trudeau, L. Lickley, C. Holloway, D. R. McCready, D. Maclean and A. Marks, Enumeration of circulating tumor cells in the blood of breast cancer patients after filtration enrichment: correlation with disease stage, *Breast Cancer Res. Treast.*, 2004, **86**, 237–247.
10 J. B. Smerage and D. F. Hayes, The measurement and therapeutic implications of circulating tumor cells in breast cancer, *Br. J. Cancer*, 2006, **94**, 8–12.
11 W. C. Chang, L. P. Lee and D. Liepmann, Biomimetic technique for adhesion-based collection and separation of cells in a microfluidic channel, *Lab Chip*, 2005, **5**, 64–73.
12 X. Cheng, D. Irimia, M. Dixon, K. Sekine, U. Demirci, L. Zamir, R. G. Tompkins, W. Rodriguez and M. Toner, A microfluidic device for practical label-free CD4+ T cell counting of HIV-infected subjects, *Lab Chip*, 2007, **7**, 170–178.
13 B. D. Plouffe, M. Radisic and S. K. Murthy, Microfluidic depletion of endothelial cells, smooth muscle cells, and fibroblasts from heterogeneous suspensions, *Lab Chip*, 2008, **8**, 462–472.
14 Z. Du, K. H. Cheng, M. W. Vaughn, N. L. Collie and L. S. Gollahon, Recognition and capture of breast cancer cells using a antibody-based platform in a microelectromechanical systems device, *Biomed. Microdevices*, 2007, **9**, 35–42.
15 S. Nagrath, L. V. Sequist, S. Maheswaran, D. W. Bell, D. Irimia, L. Ulkus, M. R. Smith, E. L. Kwak, S. Digumarthy, A. Muzikansky, P. Ryan, U. J. Balis, R. G. Tompkins, D. A. Haber and M. Toner, Isolation of rare circulating tumor cells in cancer patients by microchip technology, *Nature*, 2007, **450**, 1235–1239.
16 P. T. Went, A. Lugli, S. Meier, M. Bundi, M. Mirlacher, G. Sauter and S. Dirnhofer, Frequent EpCam protein expression in human carcinomas, *Hum. Pathol.*, 2004, **35**, 122–128.
17 M. Balzar, M. J. Winter, C. J. de Boer and S. V. Litvinov, The biology of the 17-1A antigen (Ep-CAM), *J. Mol. Med.*, 1999, **77**, 699–712.
18 B. P. L. Wijnhoven, W. N. M. Dinjens and M. Pignatelli, E-cadherin-catenin cell-cell adhesion complex and human cancer, *BJS*, 2000, **87**, 992–1005.
19 N. L. Tran, R. B. Nagle, A. E. Cress and R. L. Heimark, N-Cadherin expression in human prostate carcinoma cell lines: An epithelial-mesenchymal transformation mediating adhesion with stromal cells, *AJP*, 1999, **155**(3), 787–798.
20 H. Peinado, D. Olmeda and A. Cano, Snail, ZEB and bHLH factors in tumour progression: an alliance against the epithelial phenotype?, *Nat Rev Cancer*, 2007, **7**, 415–428.
21 G. Agiostratidou, J. Hulit, G. R. Phillips and R. B. Hazan, Differential cadherin expression: potential markers for epithelial to mesenchymal transformation during tumor progression, *J. Mammary Gland Biol. Neoplasia*, 2007, **12**, 127–133.
22 X. Zhang, P. Jones and S. J. Haswell, Attachment and detachment of living cells on modified microchannel surfaces in a microfluidic-based lab-on-a-chip system, *Chem. Eng. J.*, 2008, **135S**, S82–S88.
23 D. Leckband and A. Prakasam, Mechanism and dynamics of cadherin adhesion, *Annu. Rev. Biomed. Eng.*, 2006, **8**, 259–287.
24 R. Merkel, P. Nassoy, A. Leung, K. Ritchie and E. Evans, Energy landscapes of receptor-ligand bonds explored with dynamic force spectroscopy, *Nature*, 1999, **397**, 50–53.
25 R. Alon, D. A. Hammer and T. A. Springer, Lifetime of the P-selectin-carbohydrate bond and its response to tensile force in hydrodynamic flow, *Nature*, 1995, **374**, 539–542.
26 P. Panorchan, M. S. Thompson, K. J. Davis, Y. Tseng, K. Konstantopoulos and D. Wirtz, Single-molecule analysis of cadherin-mediated cell-cell adhesion, *J. Cell Sci.*, 2006, **119**, 66–74.
27 C. Zhu, G. Bao and N. Wang, Cell mechanics: mechanical response, cell adhesion and molecular deformation, *Annu. Rev. Biomed. Eng.*, 2000, **2**, 189–226.

28 C. T. Lim, E. H. Zhou and S. T. Quek, Mechanical models for living cells–a review, *J. Biomech.*, 2006, **39**, 195–216.
29 L. Cheng, X. Xia, W. Yu, L. E. Scriven and W. W. Gerberich, Flat-punch indentation of viscoelastic material, *J. Polymer Sci.*, 2000, **38**, 10–22.
30 G. W. Schmid-Schönbein, K.-L. P. Sung, H. Tōzeren, R. Skalak and S. Chien, Passive mechanical properties of human leykocytes, *Biophys. J.*, 1981, **36**, 243–256.
31 M. Sato, D. P. Theret, L. T. Wheeler, N. Ohshima and R. M. Nerem, Application of the micropipette technique to the measurement of cultured porcine aortic endothelial cell viscoleastic properties, *J. Biomech. Eng.*, 1990, **112**, 263–268.
32 M. Sato, N. Ohshima and R. M. Nerem, Viscoelastic properties of cultured porcine aortic endothelial cells exposed to shear stress, *J. Biomech.*, 1996, **29**(4), 461–467.
33 D. P. Theret, M. J. Levesque, M. Sato, R. M. Nerem and L. T. Wheeler, The application of a homogeneous half-space model in the analysis of endothelial cell micropipette measurements, *J. Biomech. Eng.*, 1988, **110**, 190–199.
34 E. J. Koay, A. C. Shieh and K. A. Athanasiou, Creep indentation of single cells, *J. Biomech. Eng.*, 2003, **125**, 334–341.
35 E. Evans, D. Berk and A. Leung, Detachment of agglutinin-bonded red blood cells, *Biophys. J.*, 1991, **59**, 838–848.
36 L. S. L. Cheung, X. J. Zheng, A. Stopa, J. Schroeder, R. L. Heimark, J. C. Baygents, R. Guzman and Y. Zohar, Attachment & detachment of prostate cancer cells in a microfluidic system, *Proceedings of the 12th International Conference on Miniaturized Systems for Chemical and Life Sciences*, San Diego, USA, 2008, 1159–1161.
37 L. S. L. Cheung, X. J. Zheng, A. Stopa, J. Schroeder, R. L. Heimark, J. C. Baygents, R. Guzman and Y. Zohar, Flow acceleration effect on cancer cell deformation and detachment, *Proceedings of the 22nd IEEE International Conference on Micro Electro Mechanical Systems*, Sorrento, Italy, 2009.
38 L. M. Lee, R. L. Heimark, J. C. Baygents and Y. Zohar, Self-aligned immobilization of proteins utilizing PEG patterns, *Nanotechnology*, 2006, **17**, S29–S33.
39 L. M. Lee, R. L. Heimark, R. Guzman, J. C. Baygents and Y. Zohar, Low melting point agarose as a protection layer in photolithographic patterning of aligned binary proteins, *Lab Chip*, 2006, **6**, 1080–1085.
40 D. Palmieri, Q. R. Smith, P. R. Lockman, J. Bronder, B. Gril, A. F. Chambers, R. J. Weil and P. S. Steeg, Brain Metastases of Breast Cancer, *Breast Dis.*, 2006–2007, **26**, 139–147.
41 T. Yoneda, T. Michigami, B. Yi, P. J. Williams, M. Niewolna and T. Hiraga, Actions of bisphosphonate on bone metastasis in animal models of breast carcinoma, *Cancer*, 2000, **88**(S12), 2979–2988.
42 J. Hemperly, private communication, 2008.
43 I. M. Basalo, N. O. Chahine, M. Kaplun, F. H. Chen, C. T. Hung and G. A. Ateshian, Chondroitin sulfate reduces the friction coefficient of articular cartilage, *J. Biomech.*, 2007, **40**(8), 1847–1854.
44 J. Cao, B. Donel, Daniel R. Deaver, M. B. Lawrence and C. Dong, In vitro side-view imaging technique and analysis of human T-leukemic cell adhesion to ICAM-1 in shear flow, *Microvasc. Rec.*, 1998, **55**, 124–137.

Proceedings of the 2009 ASME International Mechanical Engineering Congress and Exposition
IMECE2009
November 13-19, 2009, Lake Buena Vista, Florida, USA

DRAFT

IMECE2009-13217

SPECIFIC BINDING OF CANCER CELLS USING A MICROCHAMBER FUNCTIONALIZED WITH ANTIBODIES

X.J. Zheng
Dept. of Aerospace and Mechanical Engineering
University of Arizona, Tucson, AZ, USA

L.S.L. Cheung
Dept. of Aerospace and Mechanical Engineering
University of Arizona, Tucson, AZ, USA

L. Wang
Dept. Chemical and Environmental Engineering
University of Arizona, Tucson, AZ, USA

J.A. Schroeder
Dept. Molecular and Cellular Biology
University of Arizona, Tucson, AZ, USA

R.L. Heimark
Dept. Surgery
University of Arizona, Tucson, AZ, USA

J.C. Baygents
Dept. Chemical and Environmental Engineering
University of Arizona, Tucson, AZ, USA

R. Guzman
Dept. Chemical and Environmental Engineering
University of Arizona, Tucson, AZ, USA

Y. Zohar
Dept. of Aerospace and Mechanical Engineering
University of Arizona, Tucson, AZ, USA

ABSTRACT
Specific binding of target suspended metastatic cancer cells to an antibody-functionalized surface utilizing a microfluidic device has experimentally been investigated under various conditions. The microfluidic devices, fabricated in silicon using DRIE process, consisted of a 5×5 micochamber array; each 1mm×1mm in area, and 50μm in depth. The oxide surface of the microchammber array was functionalized with various antibodies immobilized on a protein G layer. The microfluidic device design allows accurate counting of cells loaded into each microchamber and, thus, enabling a reliable counting of cells captured from homogeneous suspensions. The effects of cell suspension concentration, incubation times and ambient temperature on cell capture efficiency have been examined. Furthermore, to evaluate the specificity of the cell-surface interaction, several cell cancer types expressing different membrane receptors have been incubated on surfaces functionalized with various counter receptors. Specific binding of up to 100% of the suspended cells is observed when using surfaces functionalized with counter receptors matching the cell receptors; otherwise, non-specific binding of less than 15% of suspended cells is obtained if the functionalized counter receptors do not match the cell receptors.

1. INTRODUCTION

Circulating tumor cells have been identified in peripheral blood from cancer patients and are probably the origin of intractable metastatic disease [1]. These tumor cells are very rare, comprising as few as one cell per 10^9 cells in the blood of patients with metastatic cancer; hence, their isolation presents a tremendous technical challenge [2]. Nonetheless, these cells represent a potential alternative to invasive biopsies as a source of tumor tissue for the detection, characterization and monitoring of non-haematologic cancers [3]. The ability to identify, isolate and molecularly characterize circulating tumor cells subpopulations could further the discovery of cancer stem cell biomarkers and enhance the understanding of the biology of metastasis. Current strategies for isolating cancer cells circulating in the blood stream are still limited to complex analytic approaches that generate very low yield and purity [4].

Fluidic microsystems provide unique opportunities for cell sorting and rare-cell detection; they have been used for microfluidic flow cytometry, continuous size-based separation, and adhesion-based separation [5]. Despite their success in manipulating minute amounts of simple liquids in microscale channels, they have thus far shown

limited capability to deal with the cellular and fluid complexity of large volumes of whole blood samples [6]. Recently, the capture of tumor cells has been demonstrated using an antibody-based platform in a microdevice [7]. Micro-channels have been functionalized with anti-epithelial-cell-adhesion molecule (anti-EpCAM) antibodies to generate capture surfaces for collection of target cells [8]. In a landmark study, using the same EpCAM antibody coating, a microchannel with microposts has been developed for selective separation of viable circulating tumor cells from peripheral whole blood samples [9]. The microdevices identified tumor cells in the peripheral blood of patients with metastatic cancer with approximately 50% purity. Furthermore, the chip was utilized in monitoring changes in tumor cells number due to anti-cancer therapy; thus, providing a new and effective tool for accurate identification and measurement of tumor cells in cancer patients. Following a similar approach, we report selective binding of tumor cells in a microfluidic device coated with antibodies specific to target cell. By this method, we could distinguish different cancer cells.

2. EXPERIMENTAL ARRANGEMENTS

The interaction between cells and antibody-functionalized surfaces is a complicated process depending on numerous parameters. In order to exercise better control over several key variables, a microfluidic device consisting of a 5×5 microchamber array has been designed as sketched in Figure 1. The tight tolerance of each microchamber volume provides a convenient tool for counting biding events under fine-controlled conditions.

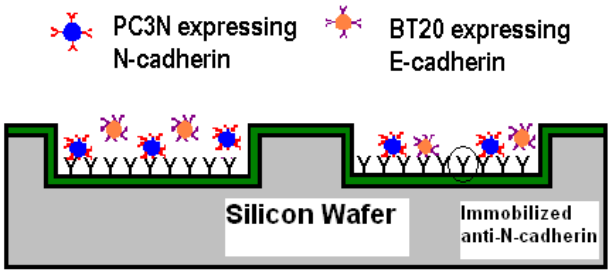

Figure 1, A schematic device cross-section designed for the capture of target cancer cells in a microchamber array functionalized with antibodies.

2.1 Device Fabrication

The fabrication starts with thermal growth and patterning of a 3000Å-thick oxide on a silicon wafer, 500μm in thick, to serve as a mask for the Deep Reactive Ion Etching (DRIE) process. The oxide film is stripped away after etching a 5×5 chamber array; each chamber is 50μm in depth and 1mm×1mm in area. The substrate is then re-oxidized to form a 3000Å-thick oxide layer to serve as a seed layer immobilizing antibodies. A photograph of a fabricated microchamber array is shown in Figure 2.

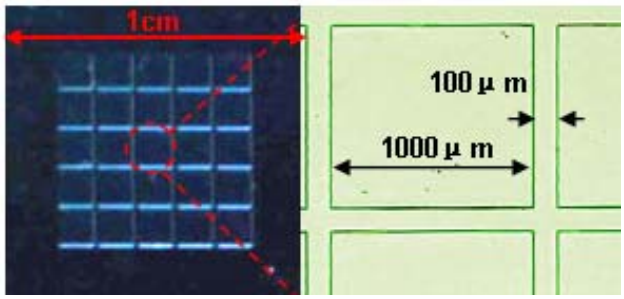

(a) (b)

Figure 2, (a) A photograph of a fabricated microdevice, and (b) An enlarged image of a single chamber 1000x1000μm^2, in area and 50μm in depth; the width of the separation wall is 100μm.

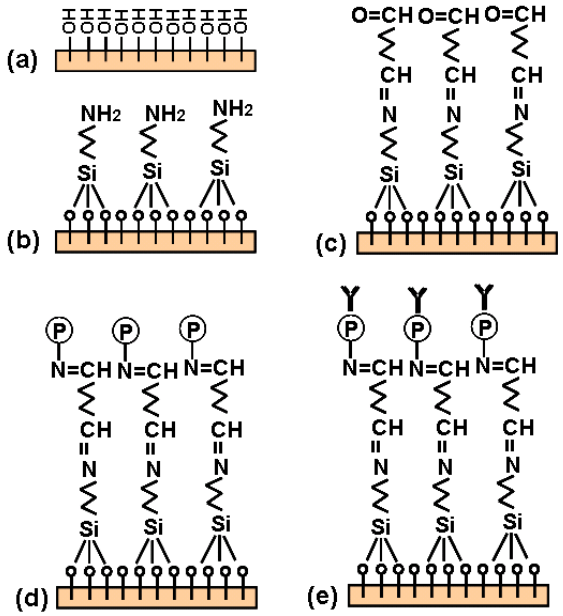

Figure 3, A schematic illustration of the immunoassay for antibody immobilization on an oxide surface.

The oxide surface of the fabricated chamber array is functionalized with a bio active layer [10], and a schematic illustration of the immunoassay is shown in Figure 3 [11]. The hydroxyl groups are silanated in 1% (vol./vol.) 3-aminopropyltriethoxysilane (APTES from Sigma) - acetone solution for 30 minutes at room temperature. The APTES-coated surface is activated with 2% (vol/vol) glutaraldehyde (Sigma) in water for 2 hours at room temperature to promote a Schiff-base reaction. Recombinant protein G from *E. coli* (Zymed Lab Inc.) 50 μg/ml in Ca- and Mg-free phosphate-buffered saline (CMF-PBS), is incubated on the activated surface for 3 hours at 4ºC. In order to block excess of silane sites, bovine serum albumin (BSA from Sigma) solution (2mg/ml in CMF-PBS) is incubated on the surface for 1 hour at room temperature. Various antibodies, at 100 μg/ml in CMF-PBS, are finally incubated on the protein G

layer at room temperature for 1 hour. The antibodies used in this work include anti-N-cadherin (IgG1, clone GC-4 from mouse, Sigma), anti-E-Cadherin (from mouse, Invitrogen), and mouse IgG (Sigma).

The surface bio-activity is tested by incubating the surfaces in anti-mouse IgG conjugated with Cy3 fluorescent dyes (Jackson ImmunoResearch Lab., Inc.), at a concentration of 15μg/ml in CMF-PBS for 1 hour at room temperature in the dark. The uniform intensity of the emitted red light (the excitation and emission wavelength is 550 and 570 nm, respectively), observed under a fluorescent microscope (Nikon eclipse 80i) as shown in Figure 4, indicates a uniform antibody activity on the chamber surface.

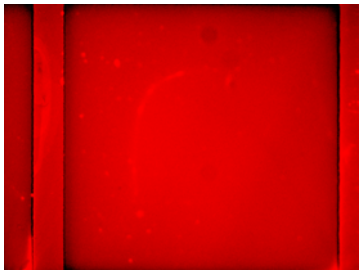

Figure 4, A fluorescent microscope image of a chamber following labeled-antigen/antibody interaction indicating uniform bioactivity of the antibody layer.

2.2 Cell Culture and Detachment

The N-cadherin expressing PC3N prostate cancer cell line [12] was grown in 1×DMEM/F12 (Dulbecco's modified Eagle's medium with 1:1 Ham's F12 medium, Invitrogen) with 10% fetal bovine serum (FBS) (Omega Scientific) and 1% penicillin-streptomycin (Cellgro). The E-cadherin expressing BT20 cell line was grown in Eagle's Minimum Essential Medium (EMEM from ATCC) with 10% FBS and 1% penicillin-streptomycin. The cadherin-11 expressing MDA-MB-231 cell line was grown maintained in RPMI 1640, with L-glutamine (Cellgro) with 10% FBS and 1% penicillin-streptomycin. All the cell lines were maintained at 37°C in 5% CO_2 in humid environment. Prior to experiments, the growth medium was aspirated and the cells were incubated with 4mM ethylenediamine-tetraacetic acid (EDTA) in CMF-PBS for 30 minutes for detachment. After centrifugation and solution removal, the cells are re-suspended in CMF-PBS. In the mixture experiment, to distinguish between cells, the cells were incubated with Celltracker (Invitrogen) 4.5uM in Dulbecco's Phosphate-Buffered Saline (D-PBS) for 30 minutes before EDTA detachment.

2.3 Cell Transfection

In order to produce a population of cells that are expressing N-cadherin, we used a vector that allows expression of N-cadherin and the cells contain fluorescent EGFP [13,14]. A plasmid was transfected into MDA-MB-231 cells and selected with neomycin. N–cadherin positive clones (Ncdh+MDA-MB-231) are characterized by expression of both GFP and N-cadherin by immunocytochemistry.

3. RESULTS AND DISCUSSION

All the cell-surface binding experiments discussed here were conducted using homogeneous cell suspensions.

3.1 Concentration and Incubation Time Effects

The effect of cell concentration and incubation time on the cell capture rate was first tested. A suspension of PC3N cells, with concentration in the range of 10^4-2.5x10^5/ml, was incubated on anti-N-cadherin functionalized micro-devices. After each certain incubation time, the devices were washed and the captured cells were counted. The incubation time includes the cell sedimentation time and cell-surface binding time. For every fixed incubation time, the area density of captured PC3N increases linearly with the suspended cell concentration as shown in figure 5(a).

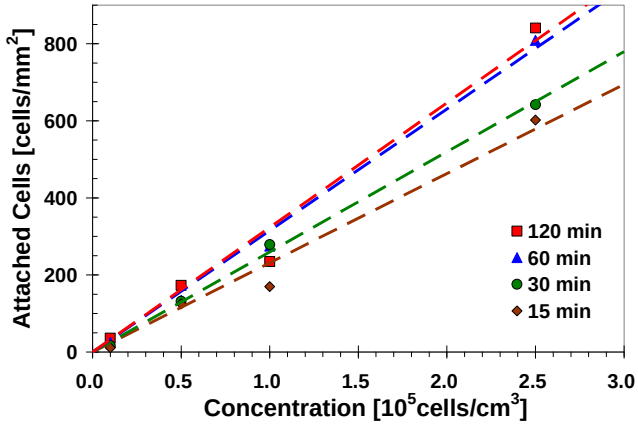

(a)

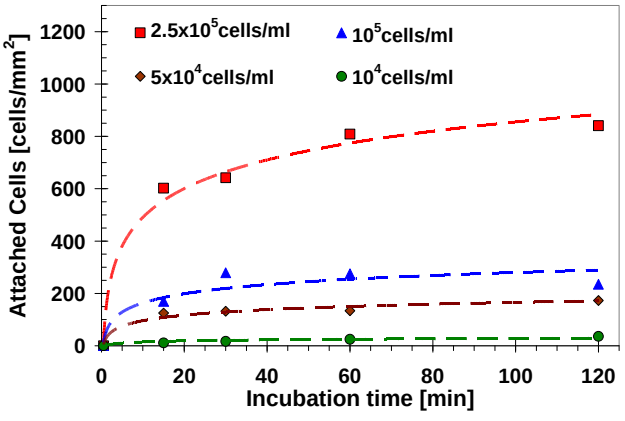

(b)

Figure 5, PC3N cell density, captured on an anti-N-cadherin functionalized surface, as a function of: (a) cell suspension concentration, and (b) incubation time.

The captured PC3N cell density is plotted in Figure 5(b) as a function of the incubation time for various cell suspension concentrations. For each given concentration, the captured cell density increases exponentially with incubation time. The asymptotic density level of the captured cells on the functionalized surface increases almost linearly with the cell-suspension concentration. Furthermore, the time constant characterizing the exponential increase in cell density also increases with the cell concentration. For example, 15min incubation time was needed for the cell density to level off for cell concentration of 10^4cells/ml, while it took about 30min incubation time for cell concentration of 10^5cells/ml.

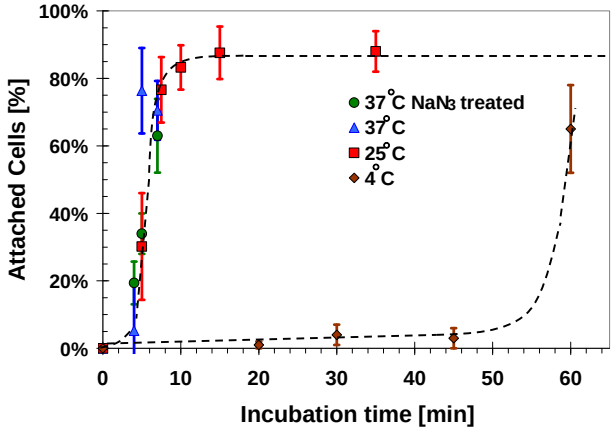

(a)

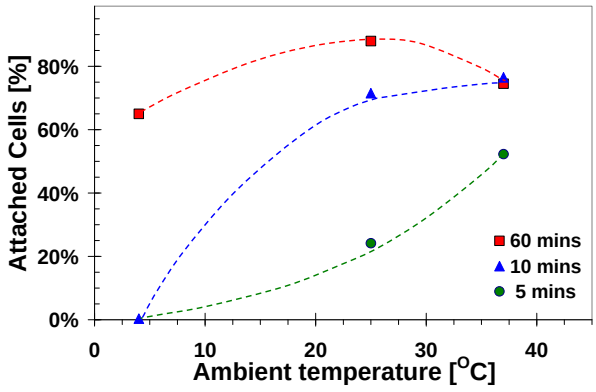

(b)

Figure 6, PC3N cell density, captured on an anti-N-cad functionalized surface, as a function of: (a) incubation time, and (b) ambient temperature.

3.2 Ambient Temperature Effect

The antigen–antibody binding is temperature-dependent [15,16]; therefore, different cell capture rates are expected under various ambient temperatures. At temperatures around 37°C, though, the immobilized antibody-cell receptor interaction could be affected by receptor internalization [17]. Thus, cells at 37°C were treated with sodium azide (NaN_3) prior to detachment to prevent receptor internalization. PC3N cell suspensions, with a fixed concentration of 10^5cells/ml, were incubated on anti-N-cadherin functionalized micro-chambers under ambient temperatures varying from 4 to 37°C. The ratio between the number of captured cells and the number of initially suspended cells, defined as the capture ratio, is plotted in Figures 6(a) and (b) as a function of the incubation time and ambient temperature, respectively. Cells without sodium azide treatment were also incubated at 37°C for comparison. The cell captured rate at 4°C ambient temperature is practically zero for an incubation time up to 45min. At higher ambient temperatures, the capture ratio is 90% after 15min incubation time. Capture ratio of 60% is obtained after 60min incubation time at 4°C. No significant difference in capture rate is observed between incubation at 25°C and 37°C, and no effect due to sodium azide treatment is detected.

3.3 Surface Coating Effect

Cell specific binding to a functionalized surface primarily depends on the surface properties. Thus far, the experimental results indicated high capture efficiency of N-cadherin expressing PC3N cancer cells, almost 100%, on an anti-N-cadherin functionalized surface. In order to test the specificity of the cell-surface interaction, identical PC3N cell suspensions ($5x10^5$cells/ml) were incubated on three surfaces with different coatings: (i) anti-N-cadherin, (ii) mouse IgG as a negative control, and (iii) SiO_2. Images of captured cells after 60min incubation time are shown in Figure 7, and the corresponding capture ratios are compared in Figure 8.

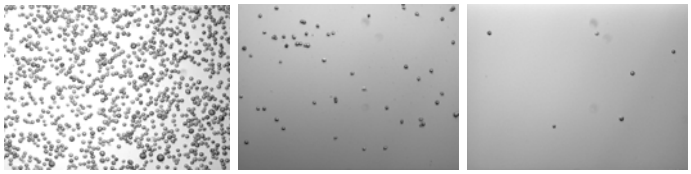

(a) (b) (c)

Figure 7, Images of PC3N cells captured from suspensions, at $5x10^5$cells/ml, on surfaces coated with: (a) anti-N-cadherin, (b) mouse IgG, and (c) SiO_2.

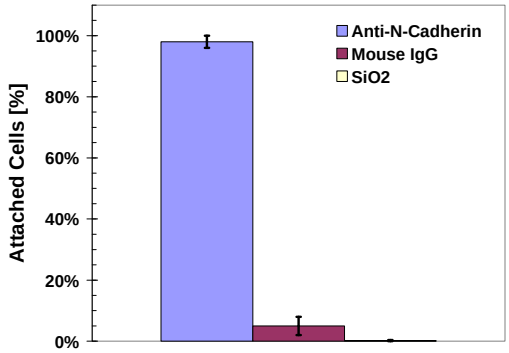

Figure 8, Measured PC3N cell capture rates for surfaces with three different coatings.

The capture rate of PC3N cell on the on the anti-N-cadherin surface is about 100%, the capture rate of the same cells on mouse IgG and SiO_2 surfaces is only 5% and 0.2%, respectively. This demonstrated that N-cadherin expressing cells have high affinity to an anti-N-cadherin functionalized surface. In order to demonstrate that this characteristic is not limited to PC3N cells, the experiments were repeated for E-cadherin expressing BT20 cancer cells. Cell suspensions, at 10^5cells/ml concentration, were incubated on surfaces functionalized with: (i) anti-E-cadherin, (ii) anti-N-cadherin, (iii) mouse IgG, and (iv) SiO_2. Images of captured cells after 60min incubation time are shown in Figure 9, and the corresponding capture rates are compared in Figure 10. Indeed, high capture rate of nearly 100% is observed only for BT20 cell incubation on an anti-E-cadherin surface, while the rate over other surfaces is less than 10%. Thus, a functionalized anti-N-cadherin surface binds with high selectivity only N-cadherin expressing cells.

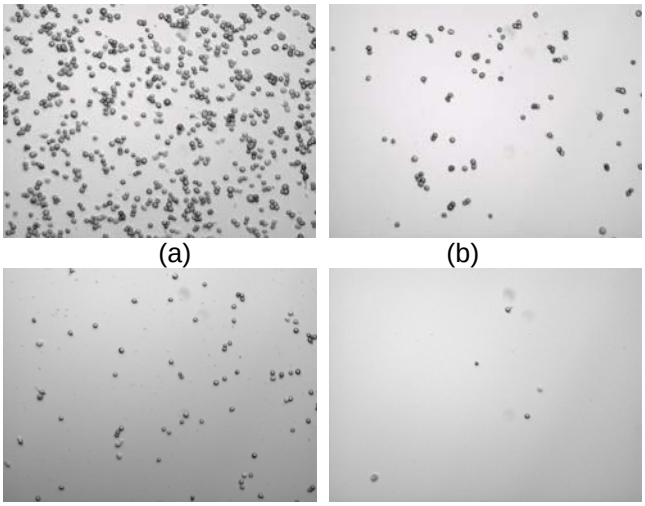

Figure 9, Images of BT20 cells captured from 10^5cells/ml suspensions on surfaces coated with: (a) anti-E-cadherin, (b) anti-N-cadherin, (c) mouse IgG, and (d) SiO_2.

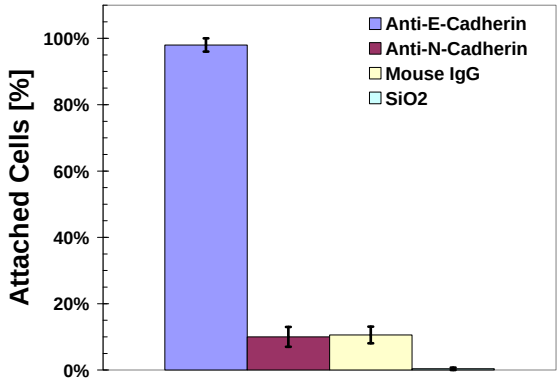

Figure 10, Measured BT20 cell capture rates on surfaces with four different coatings.

3.4 Cell Type Effect

The selectivity of binding target cells only on a certain functionalized surface was investigated using different cell types on similarly treated surfaces. Suspensions, at the same concentration of 10^5cells/ml, of three cancer cell types: (i) N-cadherin expressing PC3N, (ii) E-cadherin expressing BT20, and (iii) Cadherin-11 expressing MDA-MB-231 cells, have been incubated for 60min on anti-N-cadherin functionalized surfaces. Images of the captured cells after washing are shown in Figure 11, and the corresponding capture rates are plotted in Figure 12. Clearly, about 100% of the N-expressing PC3N cells were captured, while about 10% and only 1% of the MDA-MB-231 and BT20 cells were respectively captured. This confirms that not only the anti-N-cadherin functionalized surface has high affinity to N-cadherin expressing cells, but it also has very low affinity to other cancer cells expressing receptors different from N-cadherins.

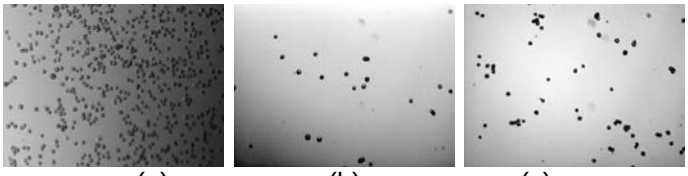

Figure 11, Images of three different cell types: (a) PC3N, (b) BT20, and (c) MDA-MB-231 captured on anti-N-cadherin functionalized surfaces (concentration 10^5cells/ml).

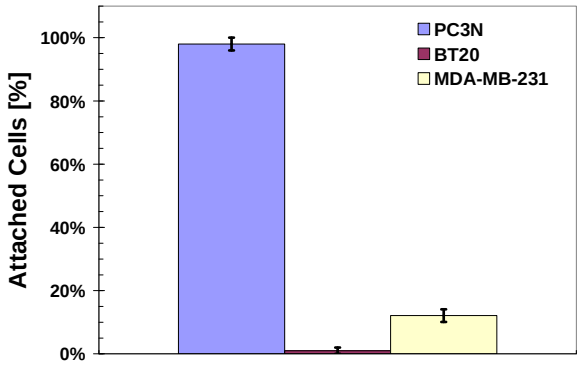

Figure 12, Capture rates of different cell lines on anti-N-cadherin surfaces.

In studying the effect of cell type on specific binding to a functionalized surface, changing the cell type is necessarily accompanied changes in other cell properties. Thus, it is important to compare binding of cells identical in all properties except their membrane receptors to categorically eliminate these modified properties as the cause for the observed poor cell affinity. MDA-MB-231 cells, normally expressing cadherin-11, were transfected with N-cadherin to perform such an experiment. Suspensions of both cell types: the

transfected Ncdh+MDA-MB-231 and parental MDA-MB-231 at a 10^5cells/ml concentration were suspended on anti-N-cadherin functionalized microchambers; incubated for 60 minutes; and washed. Images of the captured cells are shown in Figure 13, and the corresponding capture rates are compared in Figure 14. The capture rate of N-cadherin expressing cells is above 85%, while only 10% of the cadherin-11 expressing cells are captured. Hence, the high binding specificity to the functionalized surfaces is primarily due to the cell membrane receptors.

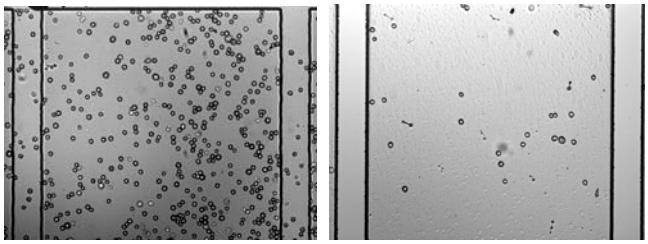

(a) (b)

Figure 13, Images of (a) Ncdh+MDA-MB-231, and (b) MDA-MB-231 cells captured on anti-N-cadherin functionalized surfaces after 60 minutes incubation time from suspensions at a concentration of 10^5cells/ml.

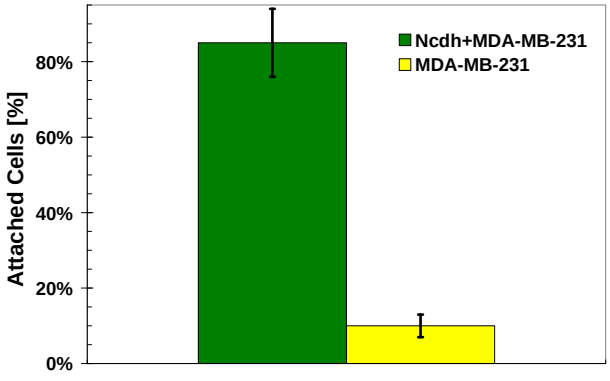

Figure 14, A comparison between the capture rates of Ncdh+MDA-MB-231 and MDA-MB-231 suspended on anti-N-cadherin surfaces.

4. CONCLUSIONS

Microchambers have been fabricated in silicon wafers, using a DRIE process, and functionalized with bio-active layers. Several parameters affecting the specificity of cell binding to the functionalized surfaces have been investigated. Specific capture of cells from suspensions increases exponentially with incubation time and linearly with concentration within the tested range. Functionalizing a surface with specific counter-receptors enables capture of almost 100% of cells with matching receptors within 15 minutes incubation time at ambient temperature higher than 25°C. Suspending cells with different receptors, changing the counter receptors immobilized on the surface, or incubation the cell suspension at low ambient temperature result in a poor capture rate.

5. ACKNOWLEDGMENTS

This work is supported by a BCRP grant, BC061859, administered by the US Army Medical Research, and the Arizona Biomedical Research Commission grant 06-080.

The full length coding region of human N-cadherin cDNA, in the vector EGFP-N1 (Clonetech) was a gift from Dr. Brian McCray (University of Arizona).

6. REFERENCES

[1] M.Cristofanilli, *et al.*, “Circulating tumor cells, disease progression, and survival in metastatic breast cancer,” *N. Engl. J. Med.*, vol. 351, pp. 781-791, 2004.

[2] H.J. Kahn, *et al.*, “Enumeration of circulating tumor cells in blood of breast cancer patients after filtration enrichment: correlation with disease stage,” *Breast Cancer Res. Treast.*, vol. 86, pp. 237-247, 2004.

[3] J.B. Smerage, *et al.*, “The measurement and therapeutic implications of circulating tumour cells in breast cancer,” *Br. J. Cancer*, vol. 94, pp. 8-12, 2006.

[4] V. Zieglschmid, *et al.* “Detection of disseminated tumor cells in peripheral blood,” *Crit. Rev. Clin. Lab. Sci.*, vol. 42, pp. 155-196, 2005.

[5] W.C. Chang, *et al.*, “Biomimetic technique for adhesion-based collection and separation of cells in a microfluidic channel,” *Lab Chip*, vol. 5, pp. 64-73, 2005.

[6] M. Toner and D. Irimia, “Blood-on-a-chip,” *Annu. Rev. Biomed. Eng.*, vol. 7, pp. 77-103, 2005.

[7] Z. Du, *et al.*, “Recognition and capture of breast cancer cells using an antibody-based platform in a microelectromechanical systems device,” *Biomed. Microdevices*, vol. 9, pp. 35-42, 2007.

[8] T. Park, *et al.*, “Capture of very rare circulating tumor cells for human breast cancer diagnosis,” *Proc. IMECE2007*, IMECE2007-42425, 2007.

[9] S. Nagrath, *et al.*, “Isolation of rare circulating tumour cells in cancer patients by microchip technology,” *Nature*, vol. 450, pp. 1235-1239, 2007.

[10] R. Iwama, *et al.*, “Fabrication of microchannels with patterned bio-active layers,” *Proc. MEMS2007*, pp. 333-336, 2007.

[11] L.M Lee, *et al.*, “Low melting point agarose as a protection layer in photolithographic patterning of aligned binary proteins,” *Lab Chip*, vol. 6, pp. 1080-1085, 2006.

[12] N. L. Tran, *et al*., “N-cadherin expression in human prostate carcinoma cell lines: An epithelial-mesenchymal transformation mediating adhesion with stromal cells,” *Am J Pathol*, vol. 155, pp. 787-798, 1999.

[13] M. Lambert, *et al*., “Immobilized dimmers of N-cadherin-Fc chimera mimic cadherin-mediated cell contact formation: contribution of both outside-in and inside-out signals,” *J. Cell Sci*., vol. 113, pp. 2207-2219, 2000.

[14] Y.T. Chen, *et al.*, “Continuous production of soluble extracellular domain of a type-I transmembrane protein in mammalian cells using an Epstein-Barr virus Ori-P-Based expression vector,” *Analytical Biochemistry*, vol. 242, pp. 276-278,.1996.
[15] G. Zeder-Lutz, *et al.*, “Thermodynamic analysis of antigen-antibody binding using biosensor measurements at different temperature,” *Analytical Biochemistry*, vol. 246, pp. 123-132, 1997.
[16] G.M. Brett, *et al.,* “Temperature-dependent binding of monoclonal antibodies to C hordein,” *Biochimica et Biophysica Acta*, vol. 1594, pp. 17-26.
[17] R.D. Klausner, *et al*., “Receptor-mediated endocytosis of transferring in K562 cells,” *J Biological Chemistry*, vol. 258, pp. 4715-4724, 1983.